Density Functional Calculations of CO Oxidation on Au(111) in the Presence of Water

Nathan Seth Froemming
Undergraduate Research Thesis in Chemistry
The University of Texas at Austin
August 19, 2008

Chapter 1

Density Functional Calculations of CO Oxidation on Au(111) in the Presence of Water

1.1 Introduction

In 1987, Haruta *et al.*[1] discovered that gold nanoparticles were highly catalytically active for CO oxidation ($CO + \frac{1}{2}O_2 \rightarrow CO_2$) at temperatures as low as 200 K. This result was quite remarkable considering that gold is the most noble of all transitions metals, excluding mercury, and thereby should not be particularly active toward *any* chemical reaction.[1] Haruta's discovery has since served as the motivation for a large amount of scientific research, including the experiment shown in Figure 1.1 performed by Goodman *et al.* In this experiment, the catalytic activity of titania-supported gold nanoparticles was monitored at 350 K as a function of nanoparticle size, and a peak was observed in CO oxidation reactivity for nanoparticle diameters of approximately 2-5 nm.

Interestingly, catalytic CO oxidation over gold nanoparticles requires the presence of *moisture* to proceed at appreciable rates[3, 4], and it has been postulated that water may assist in either activating the molecular oxygen or decomposing carbonates formed on the surface[4, 5]. Both of these hypotheses suggest that water is not directly involved but rather only *promotes* the oxidation of CO. A recent experiment examining the role of water in CO oxidation on gold has been performed by Mullins *et al.*[6], as shown in Figure 1.2. In this experiment, an Au(111) surface populated with atomic oxygen (^{16}O) and isotopically labeled water ($H_2^{18}O$) produces *two different types* of CO_2 ($C^{16}O^{16}O$ and $C^{16}O^{18}O$) when a molecular beam of $C^{16}O$ is impinged at low surface temperatures, indicating the direct involvment of water in CO oxidation with OH as a possible intermediate. The crux of this experiment can be seen in Figure 1.2C, and the main goal of the undergraduate research presented here is to explain these experimental results of Mullins *et al.* using density

[1] For instance, gold's chemical inertness is partly why we make jewelry out of it – gold might get dirty, but it doesn't tarnish, meaning that reactions do not take place on its surfaces.

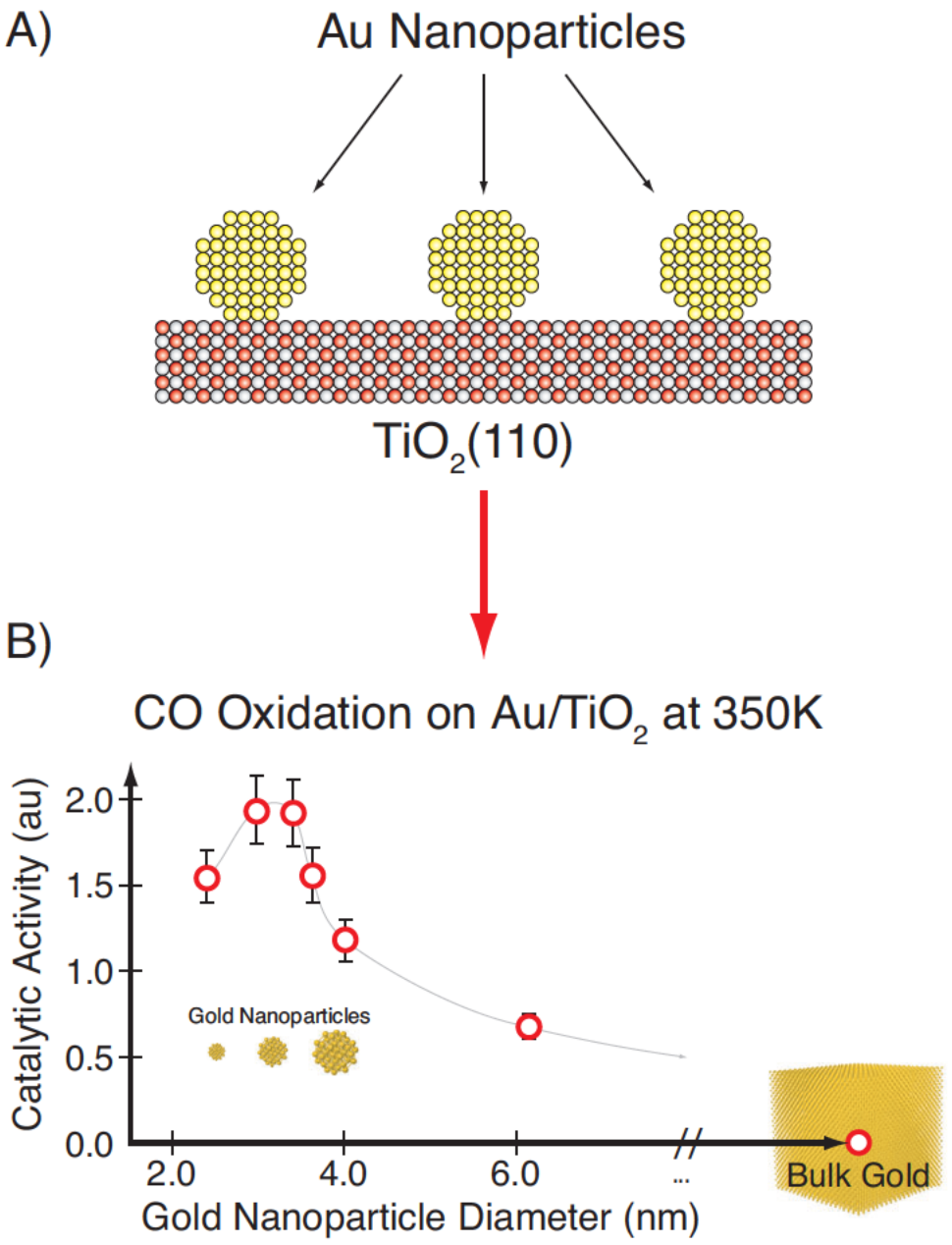

Figure 1.1: CO oxidation on gold nanoparticles at 350 K as measured by Goodman *et al.*[2]. (A) Gold nanoparticles are deposited onto a clean surface of $TiO_2(110)$, and (B) the reaction $CO + \frac{1}{2}O_2 \rightarrow CO_2$ is monitored as a function of nanoparticle size. CO oxidation proceeds most rapidly for gold nanoparticles approximately 2-5 nm in diameter. As the nanoparticles get larger, the reaction rate decreases dramatically. In the limit of large nanoparticle size, i.e. bulk gold, the reaction has completely ceased.

functional theory. One might ask, "What is the point of studying CO oxidation on Au(111) if bulk gold is catalytically *inactive* for CO oxidation?" It is well known that the {111} facet is the most stable and most prevalent configuration for a variety of metal nanoparticles, including the gold nanoparticles investigated by Haruta[1] and Goodman[2] summarized in Figure 1.1. Therefore, an understanding of CO oxidation on Au(111) may prove to be very useful in understanding CO oxidation on supported gold nanoparticles. Studying this reaction may also lend insight into the *water gas shift reaction*, $CO + H_2O \rightarrow CO_2 + H_2$, which is a part of the *steam reforming process* of hydrocarbons commonly used to generate large amounts of H_2, (e.g. $CH_4 + H_2O \rightarrow CO + 3H_2$). Lastly, CO is a poision that binds irreversibly to human heme, and so it is a worthwhile endeavor to understand ways of *getting rid of it*.[2]

1.2 Calculation Details

Calculations of the elementary steps of CO oxidation on Au(111) were performed with density functional theory (DFT) using the Perdew-Wang-91 generalized gradient approximation function[7]. The core electrons of each atom were described with pseudopotentials within the projector augmented wave framework[8] as implemented in the Vienna Ab Initio Simulation Package (VASP) code. Kohn-Sham single-electron wavefunctions were expanded in plane wave basis set up to a cutoff energy of 274.0 eV, appropriate for the pseudopotentials. Spin-polarized calculations were tested on each system and used when required. In the slab calculations, the Au(111) surface was modeled with four layers, in which the bottom two layers were frozen in the equilibrium bulk face-centered-cubic (fcc) lattice positions with a lattice constant of 4.173 Å, and the top two layers were allowed to relaxed. A vacuum gap of 10 Å was used to separate the periodic slabs. Convergence with respect to the number of layers in the slab, k-point sampling of the Brillouin Zone (BZ), and the energy cutoff for the plane wave basis set were all checked and found to be sufficient. Covereage dependence was tested by comparing a $p(2 \times 2)$ slab with four atoms per layer to a larger $p(3 \times 3)$ slab with nine atoms per layer. A Monkhorst-Pack grid[9] of $8 \times 8 \times 1$ for the $p(2 \times 2)$ slab and $4 \times 4 \times 1$ for the $p(3 \times 3)$ slab was used to sample the BZ. Energy barriers and transition states were calculated using the climbing-image nudged elastic band[10, 11] and dimer minimum-mode-following[12, 13] methods.

1.3 Results

1.3.1 The Mobility of O and CO on Au(111)

It is worth mentioning why atomic oxygen rather than molecular oxygen was used in experiments of Mullins *et al.* involving CO oxidation on Au(111) discussed above. The bottom line is that the barrier for O_2 dissociation is much higher than the binding energy of O_2 on the gold surface, and

[2]The fact that CO is not only a poison but also a byproduct of the reactions that occur in internal combustion engines necessitates the use of catalytic converters in automobile exhaust.

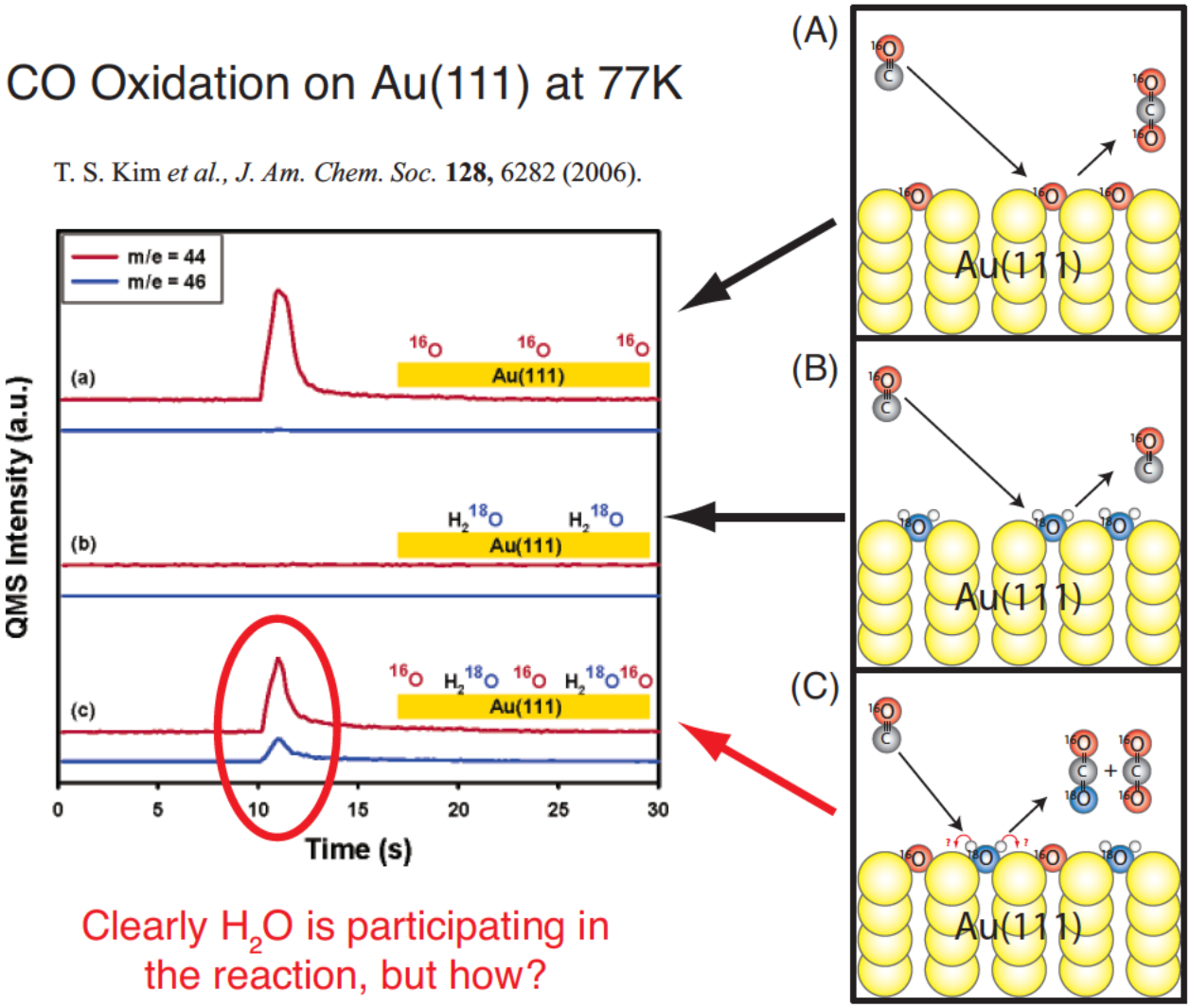

Figure 1.2: CO oxidation on atomic-oxygen-precovered Au(111) at 77 K performed by Mullin *et al.* (A) Molecular beam impingement of $C^{16}O$ on a ^{16}O-precovered Au(111) surface, in which only $C^{16}O^{16}O$ is produced. (B) Molecular beam impingement of $C^{16}O$ on a $H_2^{18}O$-precovered Au(111) surface, in which no CO_2 is produced. (C) Molecular beam impingement of $C^{16}O$ on a $H_2^{18}O$ and ^{16}O-precovered Au(111) surface, in which both $C^{16}O^{16}O$ and $C^{16}O^{18}O$ are produced, indicating that water is somehow activated by the oxygen atoms on the gold surface. In all cases, the surface precoverages of ^{16}O and $H_2^{18}O$ were 0.18 and 0.10 monolayers, respectively. The red curve in the QMS signal at the left represents $C^{16}O^{16}O$ production and the blue cure represents $C^{16}O^{18}O$ production as a function of time after the molecular beam impingement of $C^{16}O$.

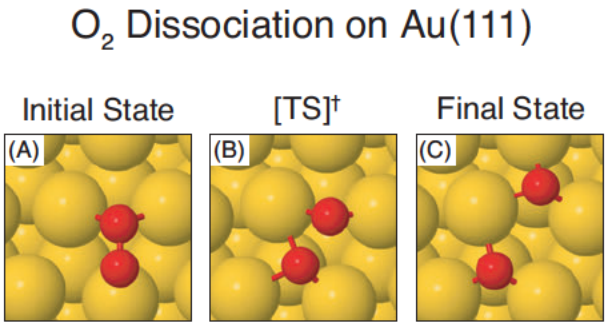

Figure 1.3: The dissociation of O_2 on Au(111) as calculated by DFT. (A) The initial state of the reaction, in which an O_2 molecule binds to a fcc site with an energy of 0.19 eV. The fcc site is the most stable binding site for O_2 on Au(111). (B) The transition state of the reaction. (C) The final state of the reaction, in which two oxygen atoms occupy hcp sites on the Au(111) surface. The barrier for this process is 0.77 eV, much higher than the binding energy of O_2 on the surface (0.19 eV). Thus, O_2 *desorbs before it dissociates* on Au(111), hence the experimenters' need to deposit atomic oxygen on Au(111) when monitoring CO oxidation.

so a bound O_2 molecule will *desorb before it dissociates* on Au(111). The reaction path for the dissociation of O_2 on Au(111), as calculated by DFT, is shown in Figure 1.3.

Once the experimenters have deposited atomic oxygen on Au(111) to monitor CO oxidation, the question arises whether the oxygen atoms are mobile on the Au(111) surface. The energy landscape for the migration of oxygen atoms on the gold surface is shown in Figure 1.4. As shown in this figure, not only is the binding energy for an oxygen atom greater at a fcc site greater than at the hcp site but also the barrier for diffusion from an fcc site is larger than from an hcp site. From the energy landscape shown in Figure 1.4, then, it can be inferred that oxygen atoms occupy only fcc sites at low surface coverages and low temperatures, and are not mobile on Au(111) at 77 K. It should be noted that the barrier for the *reverse* mechanism of that shown in Figure 1.3, in which two oxygen atoms occupying *fcc sites* (rather than the hcp sites as shown) recombine to form O_2, was calculated to be 1.39 eV, corresponding to a temperature of ~550 K. Ojifinni *et al.*[14] have measured O_2 desorption to take place from an O-precovered Au(111) surface near 540 K, indicating excellent agreement between experiment and theory in this instance.

The next logical question for studying CO oxidation is to ask is, "What happens when CO is introduced to the system in which O atoms are absorbed on the Au(111) surface?" First we will discuss the mobility of CO on the Au(111) surface, then we will turn to the reaction $CO^* + O^* \rightarrow CO_2$.[3] The energy landscape for the diffusion of CO on Au(111) is shown in Figure 1.5. The take-home message from this figure is that CO molecules are *incredibly mobile* on Au(111) at 77 K since the barrier for diffusion is only 0.07 eV and the binding of the initial and final states is very nearly the same. Contrary to the case of O_2, CO molecules do not desorb from the Au(111) surface before they have a chance to diffuse or react with coadsorbates (a CO molecule binds to the fcc site

[3]The asterisks indicate that the species is bound to the Au(111) surface.

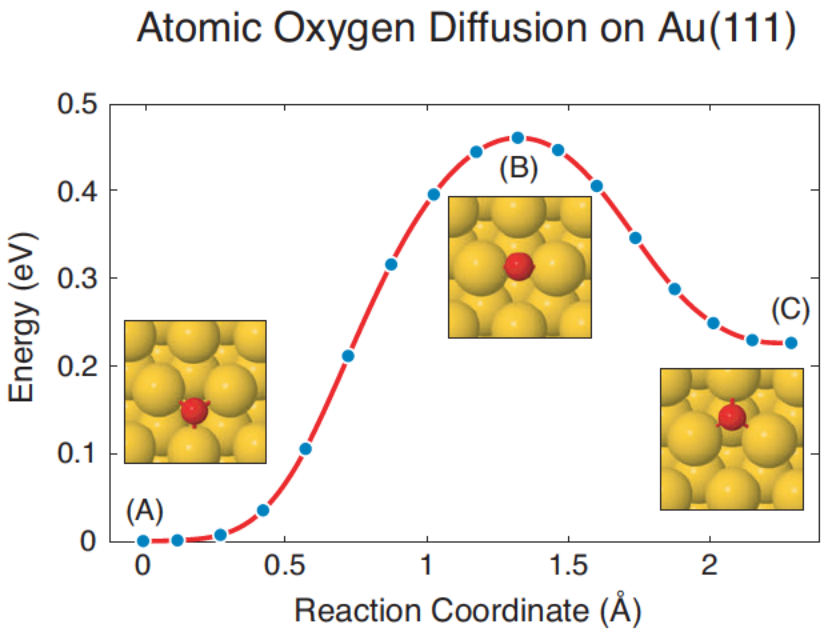

Figure 1.4: Atomic oxygen diffusion on Au(111). (A) The initial state of the reaction, in which an oxygen atom is bound to a fcc site. (B) The transition state of the reaction, corresponding to a barrier of 0.46 eV. (C) The final state of the reaction, in which the oxygen atom is bound to an hcp site. Such a process is thermally activated at ∼190 K. It should be noted that the barrier for the reverse process is only 0.20 eV (∼75 K), and that the oxygen atom prefers to occupy the fcc site over the hcp site by 0.26 eV. Hence, it can be said that, according to DFT, oxygen atoms prefer to occupy the fcc sites on Au(111) at 77 K.

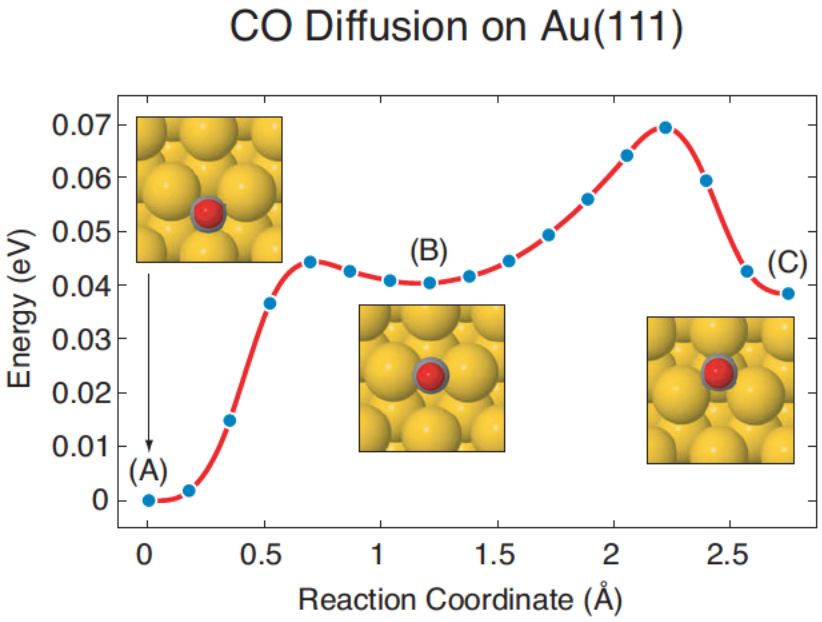

Figure 1.5: CO diffusion on Au(111). (A) The initial state of the reaction, in which a CO molecule is adsorbed to the fcc site. CO then hops through a bridging site (B) on its way to an hcp site (C). The maximum barrier encountered in this entire process is only 0.07 eV, meaning that this process is very active even at 77 K. Moreover, since the binding energies of CO at all sites at on the Au(111) surface are very near to one another, CO does not drastically prefer one site over the other, even at 77 K. Thus, CO diffusion is fast and reversible on Au(111). It should be noted that CO is bound to the surface with an energy of ~0.5 eV (depending on the binding site), and so contrary to the case of O_2, CO does not desorb from the Au(111) surface before it has a chance to diffuse or react with coadsorbates.

with an energy of 0.55 eV, corresponding to a desporption temperature of ~220 K, whereas an O_2 molecule binds to the fcc site with an energy of 0.19 eV, corresponding to a desorption temperature of ~75 K).

We are now in a position to investigate the reaction $CO^* + O^* \rightarrow CO_2$ on Au(111). Even though O atoms might be stuck in the fcc sites on the surface at 77 K, the possibility that a CO molecule might diffuse to and react with an O atom to form CO_2 exists. This process is shown in Figure 1.6. The barrier for the reaction is 0.25 eV, corresponding to a temperature of ~100 K. This calculated barrier is in reasonable agreement with the experimental observation that $CO^* + O^* \rightarrow CO_2$ occurs at temperatures as low as 77 K (recall that in these experiments, the CO molecules were bombarding the surface in a molecular beam; the kinetic energy of the CO molecules in the molecular beam is not taken into account in the calculations presented here).

1.3.2 The Role of Water in CO Oxidation

Next, we turn to the question of how exactly water participates the in oxidation of CO on Au(111). From Figure 1.2C it is clear that hydrogen atoms are transferred at some point between coadsorbed

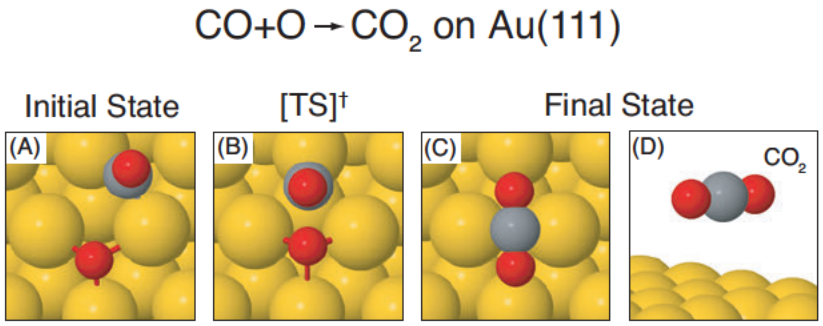

Figure 1.6: CO oxidation on Au(111). (A) The initial state of the reaction, in which a CO molecule is bound to a bridge site and an oxygen atom is bound to a fcc site. (B) The transition state of the reaction, corresponding to a barrier of 0.25 eV. (C) The final state of the reaction, in which CO_2 has completely desorbed from the Au(111) surface. (D) is simply a side view of the final state shown in (C). Such a process is thermally activated at ~100 K, in reasonable agreement with experimental observations. This reaction path is consistent with the notion that CO molecules are very mobile on the Au(111) surface whereas O atoms are essentially stuck in the fcc sites at 77 K (c.f. Figures 1.4 and 1.5).

O atoms and H_2O molecules, but when? In order to address this issue, DFT was first used to investigate whether any reaction occurred between O* and H_2O* in the *absence* of CO. The reaction of H_2O with O on Au(111) is shown in Figure 1.7. The most important thing to note from this figure is that hydrogen transfer between H_2O* and O* is both fast *and* reversible on Au(111). Figure 1.8 shows that the diffusion of OH is thermally active at ~75 K.

Finally we are in a position to address how H_2O is involved in the oxidation of CO on Au(111). Figure 1.9 shows a reaction path in which H_2O remains a spectator molecular in the reaction of CO* with O*. This is the first of three relevant reaction mechanism involving H_2O and O which leads to the formation of CO_2. We shall call the reaction shown Figure 1.9 *Mechanism I*, the most important feature of which is that hydrogen is *not transferred* between H_2O* and O* before CO oxidation takes place. It can easily be seen that this mechanism is essentially identical to that shown in Figure 1.6, with a water molecule hydrogen bonding to the oxygen atom as CO_2 is formed. The barrier for the process shown in Figure 1.9 is slightly higher than that of Figure 1.6 because of the stabilization of the initial state. Close examination of Figure 1.6B and Figure 1.9B reveals that the geometry of the transition states are essentially identical, however, since water stabilizes the initial state of Figure 1.9, the overall barrier for the reaction is slightly higher.

We have shown that the barrier CO oxidation is slightly higher when an intact water molecule is present in the reaction, but what about the reaction of CO with OH? The reaction of CO with a single OH on Au(111) is shown in Figure 1.10. This mechanism is rather complicated. First, a carboxylate intermediate must form, which has a barrier of 0.32 eV. Then, the carboxylate intermediate must undergo a *cis-trans isomerization* in which the upward-pointing hydrogen atom flips down to point toward the Au(111) surface, which has a barrier of 0.44 eV. Finally, the hydrogen atom must transfer to the surface for CO_2 to be liberated, which has a prohibitively high barrier of

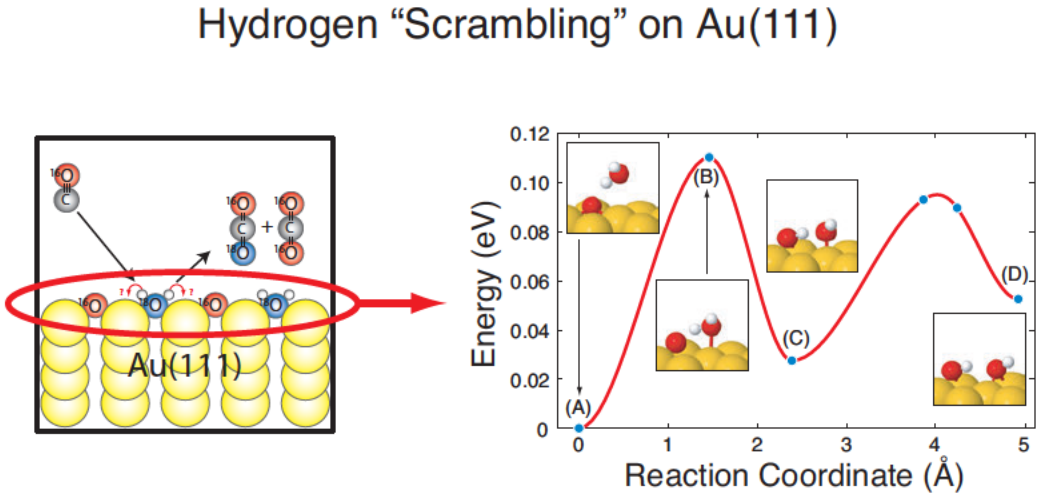

Figure 1.7: Water activation on Au(111). (A) The initial state of the reaction, in which H_2O hydrogen-bonds to an oxygen atom adsorbed at the fcc site. (B) The transition state of the reaction, corresponding to a barrier of 0.11 eV. (C) An intermediate minimum of the reaction, in which one hydroxyl resides in a bridge site while the other sits directly on top of a gold atom. (D) The final state of the reaction, in which both hydroxyls are bound in adjacent bridge sites. This process is thermally active at ~45 K. It is important to note that the low barrier and similar binding energies of the initial and final states make this reaction both fast *and* reversible on Au(111) at 77 K.

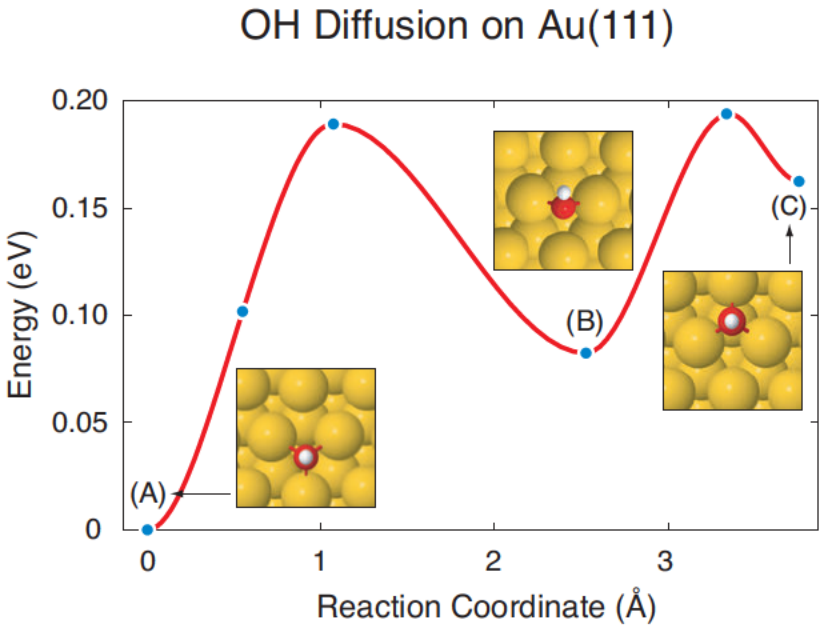

Figure 1.8: OH diffusion on Au(111). (A) The initial state of the reaction, in which OH is bound to a fcc site. (B) An intermediate minimum at a bridge site. (C) The final state of the reaction, in which OH is bound to an hcp site. The maximum barrier encountered in this reaction path is 0.19 eV, indicating that hydroxyl diffusion is thermally active at ~75 K on Au(111).

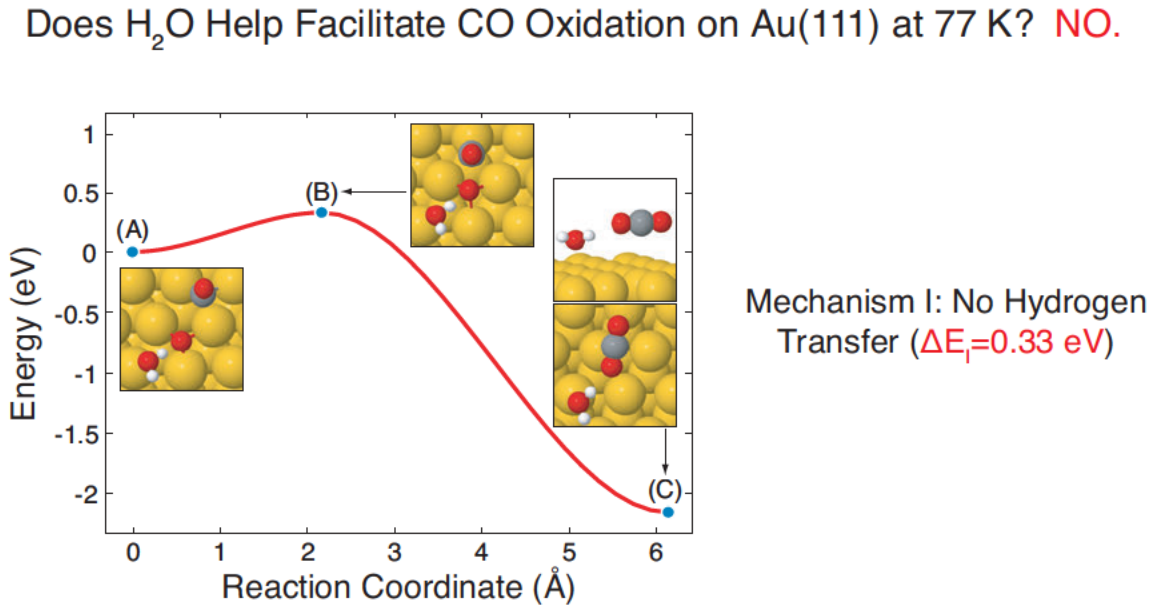

Figure 1.9: H_2O acting as a spectator molecule in the reaction of O* with CO*. (A) The initial state of the reaction, in which a water molecule hydrogen bonds to an oxygen atom adsorbed at the fcc site. (B) The transition state of the reaction, corresponding to a barrier of 0.33 eV. (C) The final state of the reaction, in which CO_2 has desorbed from the surface yet is still interacting with H_2O. It is important to note the similarities of this mechanism with the one shown in Figure 1.6. The mechanism shown above is essentially identical to that shown in Figure 1.6, only water is hydrogen bonding to the oxygen atom as CO_2 is formed. Since the initial state (A) is stabilized as a result of the hydrogen bond (c.f. Figure 1.6A), and since the transition state (B) is essentially identical to the mechanism without water (c.f. Figure 1.6B), the overall reaction barrier for the process shown above is slightly than the mechanism without water.

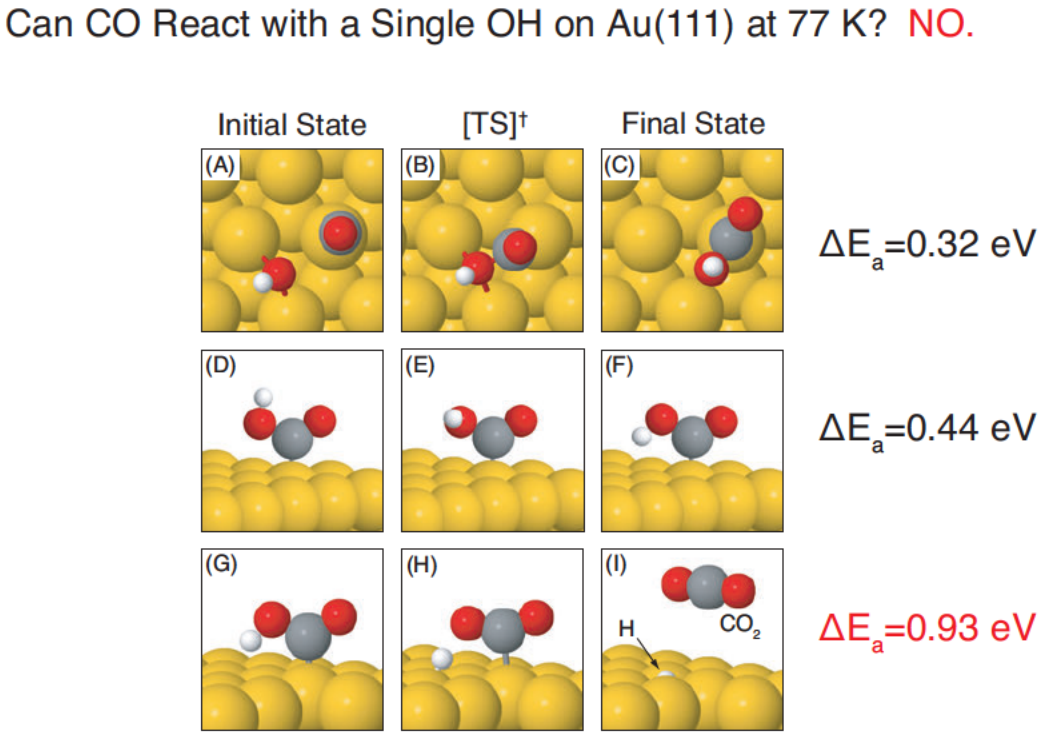

Figure 1.10: The reaction of CO with OH to form CO_2 on Au(111). (A-C) The formation of COOH* (carboxylate) intermediate. (D-F) *Cis-trans* isomerization of the carboxylate intermediate, in which the hydrogen atom flips downward to point toward the surface. The barrier for this process is 0.44 eV. (G-I) Transfer of the hydrogen atom to the Au(111) surface resulting in the liberation of CO_2. This reaction occurs with the prohibitively high barrier of 0.93 eV, corresponding to a thermal activation temperature of ~370 K. Thus, CO does not react with OH to form CO_2 on Au(111) at 77 K.

0.93 eV. The bottom line is that the reaction of CO with OH is *not a possible mechanism* in which H_2O is involved (in the form of hydroxyl) that leads to the formation of CO_2 on Au(111) at 77 K.

Since CO* reacts rather easily with OH* to form COOH* (Figure 1.10A-C), we cannot discount the possibility of COOH* reacting with some other adsorbate to form CO_2. The reaction $COOH^* + OH^* \rightarrow CO_2 + H_2O^*$ is considered in Figure 1.11. The most important thing to note about this figure is that the barrier for the reaction is 0.28 eV, which is not really any better than shown in Figure 1.6 for $CO^* + O^* \rightarrow CO_2$. Still, the reaction is thermally active at ~110 K, and could be responsible in part for the $C^{16}O^{18}O$ observed by Mullins *et al.* We shall call the pathway shown in Figure 1.11 *Mechanism II*, because it is the second relevant mechanism we have encountered involving water (in the form of hydroxyl) that leads to the formation of CO_2 at 77 K. The defining feature of Mechanism II is that hydrogen transfer has occurred *before* CO oxidation takes place, hence our dubbing of this mechanism as involving "early hydrogen transfer."

We will now discuss the last of the three relevant mechanisms involving H_2O that lead to the formation of CO_2 on Au(111) at 77 K, namely, the reaction $CO^* + 2OH^* \rightarrow CO_2 + H_2O$. This

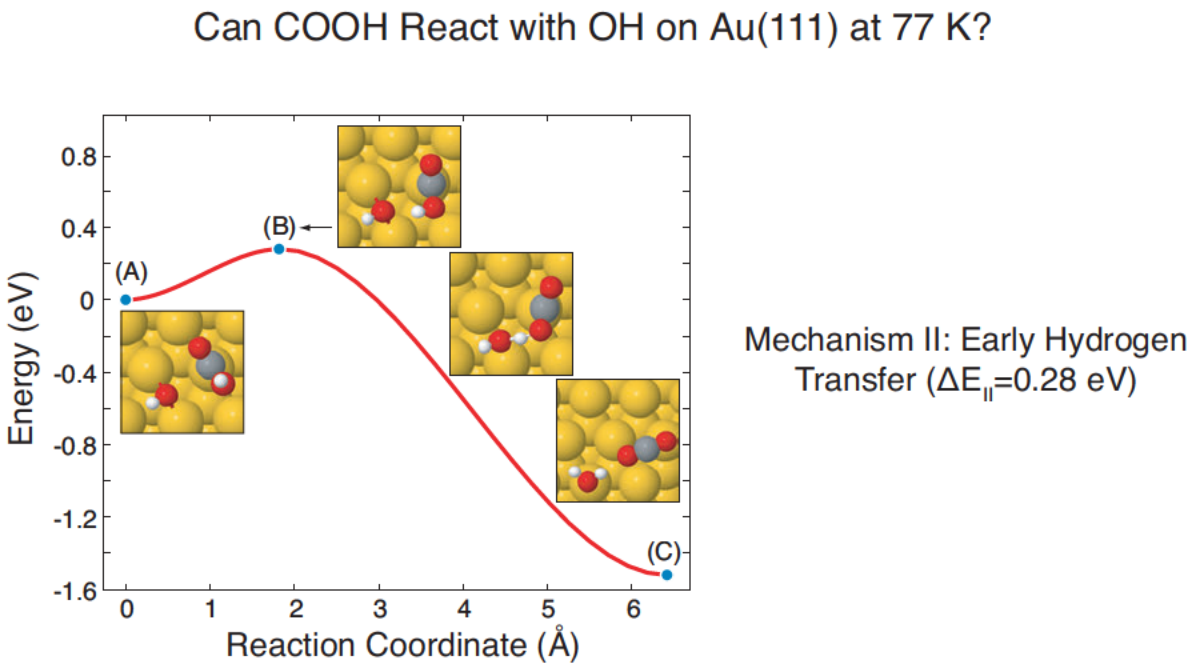

Figure 1.11: Hydrogen transfer from COOH* to OH*. (A) The initial state of the reaction, in which COOH is bound directly on top of a surface Au atom and an OH occupying a bridge site is nearby. (B) The transition state of the reaction, corresponding to a barrier of 0.28 eV. (C) The final state of the reaction, in which CO_2 has desorbed from the surface yet is still interacting with a bound H_2O molecule. This reaction path involves hydrogen transfer before CO_2 oxidation has taken place, hence the pathway's name.

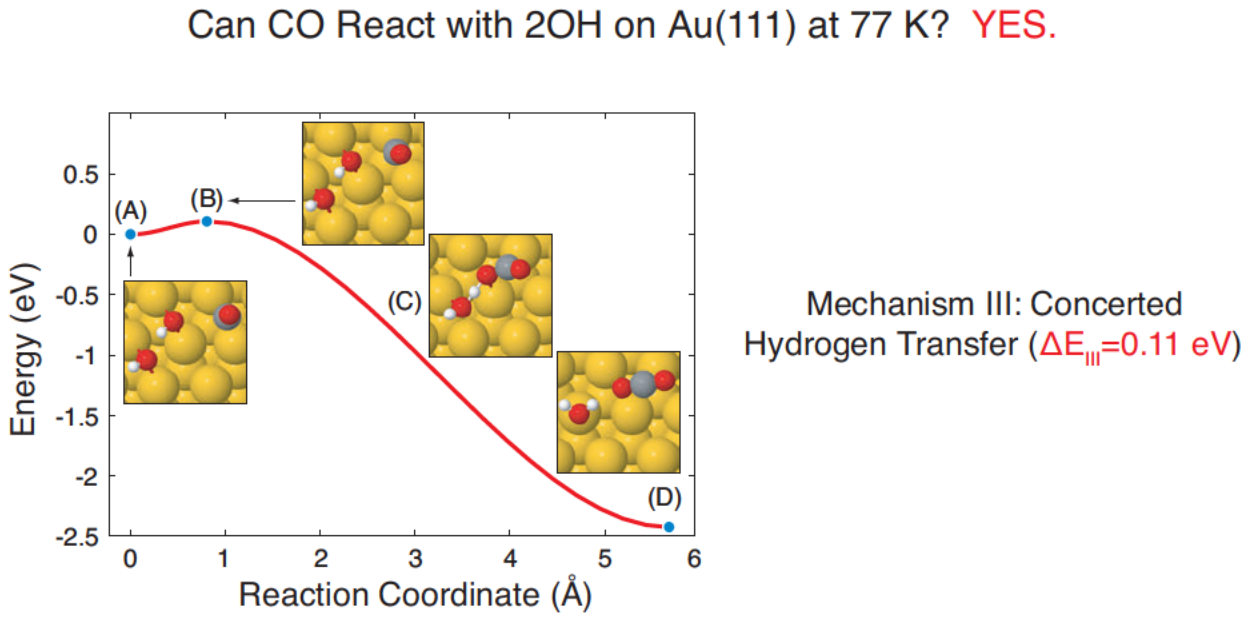

Figure 1.12: The reaction of CO* with 2OH* on Au(111). (A) The initial state of the reaction, in which two OH are hydrogen bonding via adjacent bridge sites and CO is also in an adjacent bridge site. (B) The transition state of the reaction, corresponding to a barrier of only 0.11 eV. (C) Complex OCOHOH configuration along the reaction path. (D) The final state of the reaction, in which CO_2 has desorbed from the surface yet is still interacting with a bound H_2O molecule. This process is thermally active at temperatures well below 77 K. Since this process involves the transfer of hydrogen from one OH to the other at the same time CO oxidation takes place, we call this pathway *Mechanism III: concerted hydrogen transfer*.

pathway is shown in Figure 1.12, and as can be seen in the figure, it is appropriately labeled *Mechanism III: concerted hydrogen transfer*. The barrier for the reaction is only 0.11 eV, corresponding to a thermal activation temperature of around 45 K. This is the most important mechanism of the three we have discussed since it involves such a low barrier. Ironically, both water activation (Figure 1.7) and Mechanism III occur with a barrier of 0.11 eV, both of which are necessary for H_2O to participate in CO oxidation at 77 K.

A comparison of the overall energy landscapes of Mechanisms I-III is shown in Figure 1.13. It is important to note that each of the three reaction mechanisms have CO, O, and H_2O as reactants and CO_2 and H_2O as products. From this figure it is clear that the reactants in Mechanism III do not get trapped in an intermediate potential well, hence there being such a small barrier for CO oxidation to take place. Mechanism III is entirely consistent with the experimental observation that CO oxidation readily occurs at 77 K on Au(111).

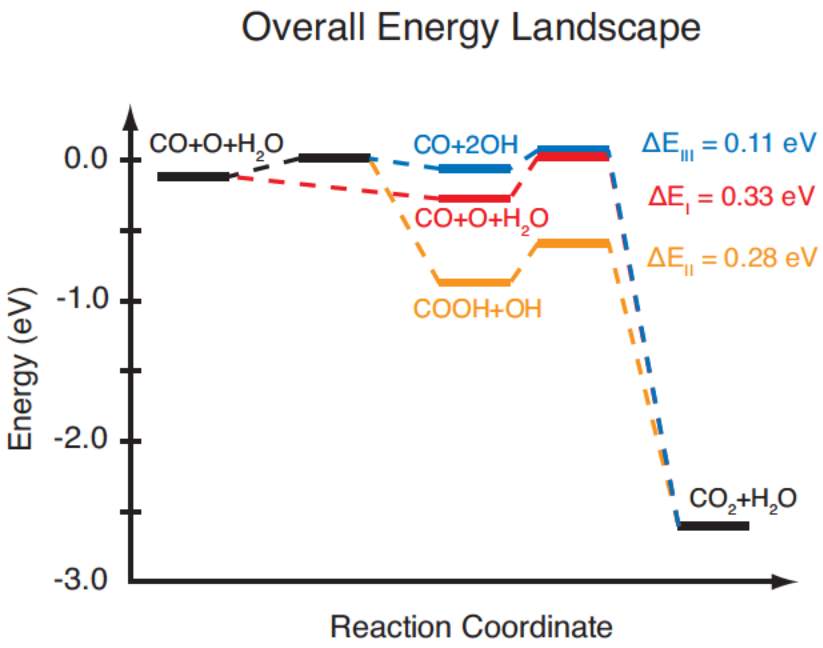

Figure 1.13: Overall energy landscape for the three reaction mechanisms of CO oxidation in the presence of H_2O. Each of the three mechanisms has the same initial and final states. In Mechanism I (red), there is no hydrogen transfer from H_2O. In Mechanism II (orange), hydrogen transfer occurs before CO oxidation takes place. In Mechanism III (blue), hydrogen transfer occurs concertedly with CO oxidation, leading to the lowest overall barrier for CO oxidation (0.11 eV). Mechanism III is entirely consistent with the experimental observation that CO oxidation readily occurs at 77 K on Au(111).

1.4 Conclusions

We have presented a set of DFT calculations that offers insight as to why water acts as a promoter for CO oxidation on Au(111). Water appears to directly react with adsorbed oxygen atoms, leading to the fast and reversible formation of OH groups on the surface. Once surface hydroxyls have formed, CO can react in a variety of ways with OH molecules to form CO_2. We have presented three possible mechanisms in which water, possibly in the form of hydroxyl, can be involved in the oxidation CO at low temperatures. One of these reaction mechanisms, Mechanism III, involves the concerted transfer of hydrogen in CO oxidation and is more than likely the reason that CO oxidation is observed to take place on Au(111) at 77 K in the presence of water. A more formal discussion of that which has been described above can be found in [14]. A natural extension of this work involving the reaction $CO_2 + \frac{1}{2}O_2 \rightarrow CO_3$ can be found in [15].

Bibliography

[1] M. Haruta, T. Kobayashi, H. Sano, and N. Yamada. *Chem. Lett.*, 16:405, 1987.

[2] C. C. Chusuei, X. Lai, K. Luo, and D. W. Goodman. *Top. Catal.*, 14:71, 2001.

[3] M. Date and M. Haruta. *J. Catal.*, 201:221, 2001.

[4] M. Date, M. Okumura, S. Tsubota, and M. Haruta. *Angew. Chem., Int. Ed.*, 43:2129, 2004.

[5] F. Boccuzzi and A. Chiorino. *J. Phys. Chem. B*, 104:5414, 2000.

[6] T. S. Kim, J. Gong, R. Ojifinni, J. M. White, and C. B. Mullins. *J. Am. Chem. Soc.*, 128:6282, 2006.

[7] J. P. Perdew. *Electronic Structure of Solids*, page 11. Akademie Verlag, Berlin, 1991.

[8] G. Kresse and D. Joubert. *Phys. Rev. B*, 59:1758, 1999.

[9] H. J. Monkhorst and J. D. Pack. *Phys. Rev. B*, 13:5188, 1976.

[10] G. Henkelman and H. Jonsson. *J. Chem. Phys.*, 113:9978, 2000.

[11] G. Henkelman, B. P. Uberuaga, and H. Jonsson. *J. Chem. Phys.*, 113:9901, 2000.

[12] G. Henkelman and H. Jonsson. *H. Chem. Phys.*, 111:7010, 1999.

[13] R. A. Olsen, G. J. Kroes, G. Henkelman, A. Arnaldsson, and H. Jonsson. *J. Chem. Phys.*, 121:9776, 2004.

[14] R. A. Ojifinni, N. S. Froemming, J. Gong, M. Pan, T. S. Kim, J. M. White, G. Henkelman, and C. B. Mullins. *J. Am. Chem. Soc.*, 130(21):6801, 2008.

[15] R. A. Ojifinni, J. Gong, N. S. Froemming, D. W. Flaherty, M. Pan, G. Henkelman, and C. B. Mullins. *J. Am. Chem. Soc.*, 130(34):11250, 2008.

[16] P. Hohenberg and W. Kohn. Inhomogeneous electron gas. *Phys. Rev.*, 136(3B), 1964.

[17] W. Kohn and L. J. Sham. Self-consistent equations including exchange and correlation effects. *Phys. Rev.*, 140(4A):A1133–A1138, 1965.

Appendix A

Matehmatical Review

A.1 The Calculus of Variations

The calculus of variations will be used to prove a very important theorem in density functional theory (§B.1), and so we present a brief review of the calculus of variations here. Suppose that we wish to minimize the integral

$$I = \int_{x_1}^{x_2} f(x, y, y')\, dx \ . \tag{A.1}$$

We denote the function that minimizes Equation (A.1) by $y(x)$ and form the one-parameter "trial" functions $\tilde{y}(x)$, defined by

$$\tilde{y}(x) = y(x) + \epsilon\eta(x) \ , \tag{A.2}$$

where $\eta(x)$ is an arbitrary differentiable function for which $\eta(x_1) = \eta(x_2) = 0$ and ϵ is a parameter of that particular family of curves. This ensures that $\tilde{y}(x_1) = y(x_1) = y_1$ and $\tilde{y}(x_2) = y(x_2) = y_2$. Thus the value of the integral (A.1) is now a function of the variable ϵ, and we are concerned with minimizing

$$I(\epsilon) = \int_{x_1}^{x_2} f(x, \tilde{y}, \tilde{y}')\, dx \ , \tag{A.3}$$

meaning that we desire

$$\frac{dI}{d\epsilon} = \int_{x_1}^{x_2} \left(\frac{\partial f}{\partial \tilde{y}} \frac{d\tilde{y}}{d\epsilon} + \frac{\partial f}{\partial \tilde{y}'} \frac{d\tilde{y}'}{d\epsilon} \right) dx \tag{A.4}$$

to be an extremum. From the definition of $\tilde{y}(x)$ in (A.2), the above equation now becomes

$$\frac{dI}{d\epsilon} = \int_{x_1}^{x_2} \left(\frac{\partial f}{\partial \tilde{y}}\, \eta(x) + \frac{\partial f}{\partial \tilde{y}'}\, \eta'(x) \right) dx \ . \tag{A.5}$$

Clearly when $\epsilon \to 0$, $\tilde{y} \to y$ and $\tilde{y}' \to y'$, so

$$\left.\frac{dI}{d\epsilon}\right|_{\epsilon=0} = \int_{x_1}^{x_2} \left(\frac{\partial f}{\partial y}\,\eta(x) + \frac{\partial f}{\partial y'}\,\eta'(x) \right) dx = 0 \,. \tag{A.6}$$

Integrating the second term in parenthesis by parts, we obtain

$$\int_{x_1}^{x_2} \frac{\partial f}{\partial y'}\,\eta'(x)\,dx = \left.\frac{\partial f}{\partial y'}\,\eta(x)\right|_{x_1}^{x_2} - \int_{x_1}^{x_2} \frac{d}{dx}\left(\frac{\partial f}{\partial y'}\right)\eta(x)\,dx \,. \tag{A.7}$$

The first term on the left is zero since $\eta(x)$ is zero at x_1 and x_2, leaving us with

$$\left.\frac{dI}{d\epsilon}\right|_{\epsilon=0} = \int_{x_1}^{x_2} \left(\frac{\partial f}{\partial y} - \frac{d}{dx}\frac{\partial f}{\partial y'} \right)\eta(x)\,dx = 0 \,. \tag{A.8}$$

Since $\eta(x)$ is arbitrary but nonzero, the integrand must be equal to zero for the relation to hold, namely

$$\boxed{\left(\frac{\partial f}{\partial y} - \frac{d}{dx}\frac{\partial f}{\partial y'} \right) = 0 \,.} \tag{A.9}$$

This important result is known as the *Euler-Lagrange equation*, which is a necessary condition for the value of the integral in Equation (A.1) to have an extremum value. It should be noted that the symbol δ was used in the early days of the development of the calculus of variations to indicate differentiation with respect to the parameter ϵ. It is analogous to the symbol d in a differential except that it warns you that ϵ and not x is the differentiation variable. Thus the quantity δI (read "the variation of I") is simply the differential

$$\delta I = \frac{dI}{d\epsilon}\,d\epsilon \,, \tag{A.10}$$

where $dI/d\epsilon$ is evaluated for $\epsilon = 0$.

Appendix B

Density Functional Theory

B.1 A Brief Review of Density Functional Theory

In the simple Born-Oppenheimer molecule, the time-independent Hamiltonian for an N-electron system is written as

$$\hat{\mathscr{H}} = T + U + V \tag{B.1}$$

where T is the kinetic energy, U is the potential between the N electrons, and V is the potential due to the external fields, i.e. the nuclear charges. If we let

$$V = \sum_{i=1}^{N} v(\mathbf{r}_i) \ , \tag{B.2}$$

the first Hohenberg-Kohn theorem[16] states that *the potential $v(\mathbf{r})$ is completely determined by the electron density $\rho(\mathbf{r})$ to within an additive constant.* To prove this theorem, we must show that there exists a one-to-one map between $v(\mathbf{r})$ and $\rho(\mathbf{r})$. Assuming a non-degenerate ground state with energy E_0, the Schrödinger equation

$$\hat{\mathscr{H}}\Psi = E_0\Psi \tag{B.3}$$

defines a mapping for each $v(\mathbf{r})$ to the ground state wavefunction Ψ, and from this wavefunction we can find the ground state density $\rho(\mathbf{r})$. It remains to show that two different ground states Ψ and Ψ' arising from different potentials $v(\mathbf{r})$ and $v'(\mathbf{r})$ always give rise to *different* ground state densities. Calling the corresponding Hamiltonians $\hat{\mathscr{H}}$ and $\hat{\mathscr{H}}'$, E_0 is given by

$$\begin{aligned} E_0 = \langle\Psi|\hat{\mathscr{H}}|\Psi\rangle < \langle\Psi'|\hat{\mathscr{H}}|\Psi'\rangle =& \langle\Psi'|\hat{\mathscr{H}}' - V' + V|\Psi'\rangle \\ =& E_0' + \int \rho'(\mathbf{r})[v'(\mathbf{r}) - v(\mathbf{r})]\, d\mathbf{r} \end{aligned} \tag{B.4}$$

Likewise, we can show that

$$E_0' < E_0 - \int \rho(\mathbf{r})[v'(\mathbf{r}) - v(\mathbf{r})]\, d\mathbf{r} \; . \tag{B.5}$$

Adding these two inequalities, we get

$$E_0 + E_0' < E_0' + E_0 + \int [\rho'(\mathbf{r}) - \rho(\mathbf{r})][v'(\mathbf{r}) - v(\mathbf{r})]\, d\mathbf{r} \tag{B.6}$$

By hypothesis, $v'(\mathbf{r})$ and $v(\mathbf{r})$ are different, and so their difference is nonzero. If we assume that $\rho'(\mathbf{r}) = \rho(\mathbf{r})$ we get the self-contradiction

$$E_0 + E_0' < E_0' + E_0 \; . \tag{B.7}$$

Thus, we conclude that the two different densities must correspond to two different potentials, and a non-degenerate ground state can correspond to one and only one potential.

The second Hohenberg-Kohn theorem[17] establishes a variational principle for the energy as a *functional*[1] of the density: *If* $\rho(\mathbf{r})$ *is the density arising from the solution of the* N*-electron Schrödinger equation*

$$\hat{\mathscr{H}}\Psi = E[\rho]\Psi \; , \tag{B.8}$$

then for any density $\rho'(\mathbf{r}) \neq \rho(\mathbf{r})$ *that satisfies*

$$\int \rho(\mathbf{r})\, d\mathbf{r} = N \; , \tag{B.9}$$

we must have $E[\rho'] > E[\rho]$. This theorem follows readily from the one-to-one correspondence between Ψ and $\rho(\mathbf{r})$. By incorporating the N-electron constraint on the density using a Lagrangian multiplier λ, we can formulate the stationary condition at the minimum as

$$\delta \left[E[\rho] - \lambda \left(\int \rho(\mathbf{r})\, d\mathbf{r} - N \right) \right] = 0 \; . \tag{B.10}$$

Substituting for the energy functional in this expression,

$$\begin{aligned} E[\rho] = \langle \Psi | \hat{\mathscr{H}} | \Psi \rangle = \langle \Psi | T + U + V | \Psi \rangle =& \langle \Psi | T + U | \Psi \rangle + \int \rho(\mathbf{r}) v(\mathbf{r})\, d\mathbf{r} \\ =& F[\rho] + \int \rho(\mathbf{r}) v(\mathbf{r})\, d\mathbf{r} \; , \end{aligned} \tag{B.11}$$

the stationary condition may be re-cast in the Euler-Lagrange form

$$\lambda = \frac{\delta E[\rho]}{\delta \rho(\mathbf{r})} = v(\mathbf{r}) + \frac{\delta F[\rho]}{\delta \rho(\mathbf{r})} \; , \tag{B.12}$$

[1] A functional is function that takes a *function* as its argument and returns a scalar.

where $F[\rho]$ is the universal functional for all systems of N particles with Coulomb interactions. While Equation (B.12) is rather simple in form, it hides the fact that the universal functional $F[\rho]$ is *not* available in explicit form. Numerous schemes have been formulated for a direct optimization of the density based on these stationary conditions. One of the most efficient approach has been to use a quasi-independent-particle approximation as formulated in the Kohn-Sham equations.

To arrive at the Kohn-Sham equations, we assume the existence of a set of orbitals $\{\phi_i(\mathbf{r}),\ i = 1, 2, ..., N\}$ such that the density may be expressed in terms of these orbitals as

$$\rho(\mathbf{r}) = \sum_{i=1}^{N} \phi_i^*(\mathbf{r})\phi_i(\mathbf{r}) \ . \tag{B.13}$$

For a set of non-interacting particles, the term U vanishes and the Hamiltonian becomes

$$\hat{\mathscr{H}} = T + V = \sum_{i=1}^{N} \left(-\frac{1}{2}\nabla_i^2 + v(\mathbf{r}_i) \right) \ . \tag{B.14}$$

The ground state of this system is described by the Slater determinant

$$\Psi = |\phi_1(\mathbf{r}_1)\phi_2(\mathbf{r}_2)\cdots\phi_N(\mathbf{r}_N)| \ , \tag{B.15}$$

where $\{\phi_i(\mathbf{r}_i),\ i = 1, 2, ..., N\}$ are each solutions of the equation

$$\left(-\frac{1}{2}\nabla_i^2 + v(\mathbf{r}_i) \right) \phi_i(\mathbf{r}_i) = \epsilon_i \phi_i(\mathbf{r}_i) \tag{B.16}$$

corresponding to the lowest N eigenvalues.

In a system of interacting electrons, the term U must be included in the Hamiltonian. A large part of this is the Coulomb interaction, and we also expect this to contain some sort of exchange interaction as well as more obscure contributions due to correlation. We define an effective single-particle potential by

$$\int v^{\text{eff}}(\mathbf{r})\rho(\mathbf{r})\, d\mathbf{r} = \int v(\mathbf{r})\rho(\mathbf{r})\, d\mathbf{r} + \frac{1}{2} \iint \frac{\rho(\mathbf{r})\rho(\mathbf{r}')}{|\mathbf{r} - \mathbf{r}'|}\, d\mathbf{r}d\mathbf{r}' + E^{\text{xc}}[\rho] \ . \tag{B.17}$$

The external potential and the direct Coulomb interaction between the charge densities are indicated in the first two terms on the right, while the third term takes care of the exchange and correlation contributions to the interaction potential. Clearly the introduction of particle interactions in the system may also influence the functional form of the kinetic energy term. It is tempting to assume that it remains the same as in the non-interacting case, however this may not necessarily be so. Thus we write the exact kinetic energy functional for the interacting systems as

$$T[\rho] = T^{\text{ni}}[\rho] + \Delta T[\rho] \ , \tag{B.18}$$

where the superscript "ni" denotes that of the non-interacting system and the last term incorporates any changes in the exact kinetic energy functional due to the electron-electron interactions. Collecting all terms, we can express the energy functional for the interacting system as

$$E[\rho] = T^{\mathrm{ni}}[\rho] + \int v(\mathbf{r})\rho(\mathbf{r})\, d\mathbf{r} + \frac{1}{2}\iint \frac{\rho(\mathbf{r})\rho(\mathbf{r}')}{|\mathbf{r}-\mathbf{r}'|}\, d\mathbf{r}d\mathbf{r}' + E^{\mathrm{xc}}[\rho]\ , \tag{B.19}$$

where the correction to the kinetic energy functional has been included in the exchange-correlation functional of the interacting system:

$$E^{\mathrm{xc}}[\rho] = E^{\mathrm{xc,i}}[\rho] + \Delta T[\rho]\ . \tag{B.20}$$

The Euler-Lagrange equation (B.12) now becomes

$$\lambda = \frac{\delta E[\rho]}{\delta\rho(\mathbf{r})} = \frac{T^{\mathrm{ni}}[\rho]}{\delta\rho} + v(\mathbf{r}) + \int \frac{\rho(\mathbf{r}')}{|\mathbf{r}-\mathbf{r}'|}\, d\mathbf{r}' + v^{\mathrm{xc}}(\mathbf{r})\ , \tag{B.21}$$

where the exchange-correlation potential is defined by

$$v^{\mathrm{xc}}(\mathbf{r}) = \frac{\delta E^{\mathrm{xc}}[\rho]}{\delta\rho(\mathbf{r})}\ . \tag{B.22}$$

We note that the last three terms of the Euler-Lagrange equation (B.22) are similar to the effective potential v^{eff} introduced in Equation (B.17) except that now we have included the correction to the kinetic energy functional. We can write the Euler-Lagrange equation as

$$\lambda = \frac{\delta T^{\mathrm{ni}}[\rho]}{\delta\rho(\mathbf{r})} + v^{\mathrm{eff}}(\mathbf{r})\rho(\mathbf{r})\ . \tag{B.23}$$

But the Euler-Lagrange equation for the non-interacting particles was

$$\lambda = \frac{\delta T^{\mathrm{ni}}[\rho]}{\delta\rho(\mathbf{r})} + v(\mathbf{r})\rho(\mathbf{r})\ , \tag{B.24}$$

and this was equivalent to the set of single-particle Schrödinger equations (B.16). By analogy we conclude that for the interacting particles we can find the orbitals from the equations

$$\left(-\frac{1}{2}\nabla^2 + v^{\mathrm{eff}}(\mathbf{r}_i)\right)\phi_i(\mathbf{r}_i) = \epsilon_i\phi_i(\mathbf{r}_i)\ . \tag{B.25}$$

These are known as the *Kohn-Sham equations*, and we note that the density derived from Equation (B.13) automatically fulfills the N-particle constraint, because the orbitals are the orthonormal solutions of an eigenvalue equation.

J|A|C|S
ARTICLES

Published on Web 04/30/2008

Water-Enhanced Low-Temperature CO Oxidation and Isotope Effects on Atomic Oxygen-Covered Au(111)

Rotimi A. Ojifinni, Nathan S. Froemming, Jinlong Gong, Ming Pan, Tae S. Kim, J. M. White,† Graeme Henkelman, and C. Buddie Mullins*

Departments of Chemical Engineering and Chemistry, Texas Materials Institute, Center for Nano- and Molecular Science and Technology, University of Texas at Austin, 1 University Station C0400, Austin, Texas 78712-0231

Received January 15, 2008; E-mail: mullins@che.utexas.edu

Abstract: Water−oxygen interactions and CO oxidation by water on the oxygen-precovered Au(111) surface were studied by using molecular beam scattering techniques, temperature-programmed desorption (TPD), and density functional theory (DFT) calculations. Water thermally desorbs from the clean Au(111) surface with a peak temperature of ∼155 K; however, on a surface with preadsorbed atomic oxygen, a second water desorption peak appears at ∼175 K. DFT calculations suggest that hydroxyl formation and recombination are responsible for this higher temperature desorption feature. TPD spectra support this interpretation by showing oxygen scrambling between water and adsorbed oxygen adatoms upon heating the surface. In further support of these experimental findings, DFT calculations indicate rapid diffusion of surface hydroxyl groups at temperatures as low as 75 K. Regarding the oxidation of carbon monoxide, if a $C^{16}O$ beam impinges on a Au(111) surface covered with both atomic oxygen (^{16}O) and isotopically labeled water ($H_2{}^{18}O$), both $C^{16}O^{16}O$ and $C^{16}O^{18}O$ are produced, even at surface temperatures as low as 77 K. Similar experiments performed by impinging a $C^{16}O$ beam on a Au(111) surface covered with isotopic oxygen (^{18}O) and deuterated water ($D_2{}^{16}O$) also produce both $C^{16}O^{16}O$ and $C^{16}O^{18}O$ but less than that produced by using ^{16}O and $H_2{}^{18}O$. These results unambiguously show the direct involvement and promoting role of water in CO oxidation on oxygen-covered Au(111) at low temperatures. On the basis of our experimental results and DFT calculations, we propose that water dissociates to form hydroxyls (OH and OD), and these hydroxyls react with CO to produce CO_2. Differences in water−oxygen interactions and oxygen scrambling were observed between $^{18}O/H_2{}^{16}O$ and $^{18}O/D_2{}^{16}O$, the latter producing less scrambling. Similar differences were also observed in water reactivity toward CO oxidation, in which less CO_2 was produced with $^{16}O/D_2{}^{16}O$ than with $^{16}O/H_2{}^{16}O$. These differences are likely due to primary kinetic isotope effects due to the differences in O−H and O−D bond energies.

Introduction

Catalysis on gold has become increasingly more studied as a result of Haruta's pioneering work on the reactivity of gold nanoparticles (NPS).[1] Since then, several studies have shed additional light on the catalytic activity of gold.[2–48] These studies have reported interesting results regarding low-temperature oxidation of carbon monoxide, propylene epoxidation, water−gas shift reaction, and selective oxidation of ammonia as well as other important surface chemical reactions. Among these, low-temperature CO oxidation is quite unique because the activity of gold catalysts cannot be matched by other metals. This low-temperature activity has generated great interest and much research in metal oxide supported gold NPS. Although it is widely accepted that gold particles 2−5 nm in diameter exhibit the greatest activity,[43] research continues on the nature of the active sites for these catalysts and on details of the reaction mechanism. Although some studies suggest that the perimeter interface of gold particles with the metal oxide support acts as the active site for CO oxidation,[2,4,37,49] others based on theory and gas-phase cluster experiments[27,31,50] point to low-coordination sites on small gold particles. The oxidation state of the active form of gold is also under debate. Some studies suggest that metallic gold[6,29] is the active form, whereas others claim oxidic gold[18,20] is responsible for gold's chemical activity. Thus, several issues are in need of resolution to fully understand CO oxidation on gold catalysts. The {111} facet is the most stable and most prevalent configuration of most supported metal NPS;

† Deceased.

(1) Haruta, M.; Kobayashi, T.; Sano, H.; Yamada, N. *Chem. Lett.* **1987**, 405.
(2) Ajo, H. M.; Bondzie, V. A.; Campbell, C. T. *Catal. Lett.* **2002**, *V78*, 359.
(3) Andreeva, D.; Idakiev, V.; Tabakova, T.; Ilieva, L.; Falaras, P.; Bourlinos, A.; Travlos, A. *Catal. Today* **2002**, *72*, 51.
(4) Bollinger, M. A.; Vannice, M. A. *Appl. Catal., B* **1996**, *8*, 417.
(5) Bond, G. C.; Thompson, D. T. *Catal. Rev.* **1999**, *41*, 319.
(6) Boyen, H. G.; Kastle, G.; Weigl, F.; Koslowski, B.; Dietrich, C.; Ziemann, P.; Spatz, J. P.; Riethmuller, S.; Hartmann, C.; Moller, M.; Schmid, G.; Garnier, M. G.; Oelhafen, P. *Science* **2002**, *297*, 1533.
(7) Chen, M. S.; Goodman, D. W. *Science* **2004**, *306*, 252.
(8) Chen, M. S.; Goodman, D. W. *Acc. Chem. Res.* **2006**, *39*, 739.
(9) Chen, M. S.; Kumar, D.; Yi, C. W.; Goodman, D. W. *Science* **2005**, *310*, 291.
(10) Choudhary, T. V.; Goodman, D. W. *Top. Catal.* **2002**, *21*, 25.
(11) Choudhary, T. V.; Goodman, D. W. *Appl. Catal. A* **2005**, *291*, 32.

therefore, an understanding of CO oxidation on Au(111) will be very useful in understanding this reaction on supported Au NPS.

This work presents both experimental results and density functional theory (DFT) calculations showing the effect of adsorbed water on CO oxidation on Au(111) precovered with atomic oxygen at temperatures as low as 77 K. The interaction of water with several clean single-crystal metal surfaces has been reported, and a number of those systems have been shown to irreversibly dissociate water.[13,52–56] Studies of coadsorbed water and oxygen on metal surfaces have also been reported. These latter investigations can be divided into two broad categories: those in which water does not dissociate in the presence of oxygen on the surface and those in which oxygen induces water dissociation. For those metal surfaces known to demonstrate water dissociation in the presence of coadsorbed oxygen, it is commonly believed that the oxygen adatom abstracts a hydrogen atom from the adsorbed water molecule to form two OH groups.[57–61] In some studies, a stable water−oxygen complex was observed to be present before forming OH groups.[62–65] In most cases, OH groups adsorbed on noble metal surfaces react with sufficient heating to form water, leaving an oxygen atom on the surface. However, unless water dissociates on the clean metal surface, OH groups that have formed from the water−oxygen interaction do not dissociate further to adsorbed hydrogen and oxygen.[66]

Although many metal surfaces exhibit oxygen-induced water dissociation, there are a few cases, including Ni(111) and Ru(0001), in which water dissociation does not occur with chemisorbed oxygen atoms on the surface.[67–72] These studies have commonly noted stabilization of the molecular water by preadsorbed oxygen as evidenced by an upward shift in the water desorption temperature, but no reaction or isotopic scrambling between water and oxygen atoms on the surface was observed. Until recently, Au(111) was also regarded as a surface upon which water did not dissociate in the presence of oxygen adatoms, and as with the other metals mentioned above, water was considered to desorb from the oxygen-covered surface without reaction, leaving the original oxygen on the surface.[25] However, in an earlier, brief account[21] of some of this work, we showed evidence suggesting that oxygen-covered Au(111) might dissociate water.

Addition of moisture in the feed stream to a high surface area supported Au/TiO_2 catalyst at atmospheric pressure is

(12) Chusuei, C. C.; Lai, X. F.; Davis, K. A.; Bowers, E. K.; Goodman, D. W.; Omary, M. A.; Rawashdeh-Omary, M. A.; Fackler, J. P.; Bagus, P. S. *Abstr. Pap.—Am. Chem. Soc.* **2000**, *220*, U237.
(13) Crowell, J. E.; Chen, J. G.; Hercules, D. M.; Yates, J. J. T. *J. Chem. Phys.* **1987**, *86*, 5804.
(14) Daniells, S. T.; Makkee, M.; Moulijn, J. A. *Catal. Lett.* **2005**, *100*, 39.
(15) Date, M.; Haruta, M. *J. Catal.* **2001**, *201*, 221.
(16) Date, M.; Okumura, M.; Tsubota, S.; Haruta, M. *Angew. Chem., Int. Ed.* **2004**, *43*, 2129.
(17) Liu, L. M.; McAllister, B.; Ye, H. Q.; Hu, P. *J. Am. Chem. Soc.* **2006**, *128*, 4017.
(18) Fu, Q.; Saltsburg, H.; Flytzani-Stephanopoulos, M. *Science* **2003**, *301*, 935.
(19) Hayashi, T.; Tanaka, K.; Haruta, M. *J. Catal.* **1998**, *178*, 566.
(20) Hodge, N. A.; Kiely, C. J.; Whyman, R.; Siddiqui, M. R. H.; Hutchings, G. J.; Pankhurst, Q. A.; Wagner, F. E.; Rajaram, R. R.; Golunski, S. E. *Catal. Today* **2002**, *72*, 133.
(21) Kim, T. S.; Gong, J.; Ojifinni, R. A.; White, J. M.; Mullins, C. B. *J. Am. Chem. Soc.* **2006**, *128*, 6282.
(22) Kim, T. S.; Stiehl, J. D.; Reeves, C. T.; Meyer, R. J.; Mullins, C. B. *J. Am. Chem. Soc.* **2003**, *125*, 2018.
(23) Kolmakov, A.; Goodman, D. W. *Catal. Lett.* **2000**, *70*, 93.
(24) Kolmakov, A.; Goodman, D. W. *Surf. Sci.* **2001**, *490*, L597.
(25) Lazaga, M. A.; Wickham, D. T.; Parker, D. H.; Kastanas, G. N.; Koel, B. E. *ACS Symp. Ser.* **1993**, *523*, 90.
(26) Lin, S. D.; Bollinger, M.; Vannice, M. A. *Catal. Lett.* **1993**, *17*, 245.
(27) Liu, Z. P.; Hu, P.; Alavi, A. *J. Am. Chem. Soc.* **2002**, *124*, 14770.
(28) Liu, Z.-P.; Jenkins, S. J.; King, D. A. *Phys. Rev. Lett.* **2005**, *94*, 196102.
(29) Lopez, N.; Norskov, J. K. *J. Am. Chem. Soc.* **2002**, *124*, 11262.
(30) Luo, K.; Kim, D. Y.; Goodman, D. W. *J. Mol. Catal. A: Chem.* **2001**, *167*, 191.
(31) Mills, G.; Gordon, M. S.; Metiu, H. *J. Chem. Phys.* **2003**, *118*, 4198.
(32) Min, B. K.; Alemozafar, A. R.; Pinnaduwage, D.; Deng, X.; Friend, C. M. *J. Phys. Chem. B* **2006**, *110*, 19833.
(33) Min, B. K.; Wallace, W. T.; Goodman, D. W. *Surf. Sci.* **2006**, *600*, L7.
(34) Mul, G.; Zwijnenburg, A.; van der Linden, B.; Makkee, M.; Moulijn, J. A. *J. Catal.* **2001**, *201*, 128.
(35) Outka, D. A.; Madix, R. J. *J. Am. Chem. Soc.* **1987**, *109*, 1708.
(36) Outka, D. A.; Madix, R. J. *Surf. Sci.* **1987**, *179*, 351.
(37) Schubert, M. M.; Hackenberg, S.; van Veen, A. C.; Muhler, M ; Plzak, V.; Behm, R. J. *J. Catal.* **2001**, *197*, 113.
(38) Schumacher, B.; Plzak, V.; Kinne, M.; Behm, R. J. *Catal. Lett.* **2003**, *V89*, 109.
(39) Stangland, E. E.; Stavens, K. B.; Andres, R. P.; Delgass, W. N. *J. Catal.* **2000**, *191*, 332.
(40) Stiehl, J. D.; Gong, J. L.; Ojifinni, R. A.; Kim, T. S.; McClure, S. M.; Mullins, C. B. *J. Phys. Chem. B* **2006**, *110*, 20337.
(41) Stiehl, J. D.; Kim, T. S.; McClure, S. M.; Mullins, C. B. *J. Am. Chem. Soc.* **2004**, *126*, 13574.
(42) Tsubota, S.; Cunningham, D. A. H.; Bando, Y.; Haruta, M. Preparation of nanometer gold strongly interacted with TiO2 and the structure sensitivity in low-temperature oxidation of CO *Preparation of Catalysts Vi*, Vol. 91; Elsevier: Amsterdam, 1995; pp 227−235.
(43) Valden, M.; Lai, X.; Goodman, D. W. *Science* **1998**, *281*, 1647.
(44) Wallace, W. T.; Min, B. K.; Goodman, D. W. *J. Mol. Catal. A* **2005**, *228*, 3.
(45) Wang, Z. L.; Gao, R. P.; Nikoobakht, B.; El-Sayed, M. A. *J. Phys. Chem. B* **2000**, *104*, 5417.
(46) Yan, Z.; Chinta, S.; Mohamed, A. A.; Fackler, J. P.; Goodman, D. W. *Catal. Lett.* **2006**, *111*, 15.
(47) Meyer, R.; Lemire, C.; Shaikhutdinov, S. K.; Freund, H. *Gold Bull.* **2004**, *37*, 72.
(48) Gong, J. L.; Ojifinni, R. A.; Kim, T. S.; White, J. M.; Mullins, C. B. *J. Am. Chem. Soc.* **2006**, *128*, 9012.
(49) Grunwaldt, J. D.; Baiker, A. *J. Phys. Chem. B* **1999**, *103*, 1002.
(50) Xu, Y.; Mavrikakis, M. *J. Phys. Chem. B* **2003**, *107*, 9298.
(51) Baltrusaitis, J.; Schuttlefield, J. D.; Zeitler, E.; Jensen, J. H.; Grassian, V. H. *J. Phys. Chem. C* **2007**, *111*, 14870.
(52) Baro, A. M.; Erley, W. *J. Vac. Sci. Technol.* **1982**, *20*, 580.
(53) Callen, B. W.; Griffiths, K ; Norton, P. R.; Harrington, D. A. *J. Phys. Chem. B* **1992**, *96*, 10905.
(54) Jiang, P.; Zappone, M. W.; Bernasek, S. L.; Robertson, J. A. *J. Vac. Sci. Technol. A* **1996**, *14*, 2372.
(55) Shao, Y.; Paul, J. *Appl. Surf. Sci.* **1993**, *72*, 113.
(56) Spitzer, A.; Luth, H. *Surf. Sci.* **1985**, *160*, 353.
(57) Au, C. T.; Carley, A. F.; Pashuski, A.; Read, S.; Roberts, M. W.; Zeini-Isfahan, A. *Springer Ser. Surf. Sci.* **1993**, *33*, 241.
(58) Bedurftig, K.; Volkening, S.; Wang, Y.; Wintterlin, J.; Jacobi, K.; Ertl, G. *J. Chem. Phys.* **1999**, *111*, 11147.
(59) Creighton, J. R.; White, J. M. *Surf. Sci.* **1984**, *136*, 449.
(60) Klaua, M.; Madey, T. E. *Surf. Sci.* **1984**, *136*, L42.
(61) Seitsonen, A. P.; Zhu, Y.; Bedurftig, K.; Over, H. *J. Am. Chem. Soc.* **2001**, *123*, 7347.
(62) Bange, K.; Madey, T. E.; Sass, J. K.; Stuve, E. M. *Surf. Sci.* **1987**, *183*, 334.
(63) Fisher, G. B.; Sexton, B. A. *Phys. Rev. Lett.* **1980**, *44*, 683.
(64) Kubota, J.; Kondo, J.; Domen, K.; Hirose, C. *Surf. Sci.* **1993**, *295*, 169.
(65) Nyberg, C.; Tengstl, C. G. *J. Chem. Phys.* **1984**, *80*, 3463.
(66) Henderson, M. A. *Surf. Sci. Rep.* **2002**, *46*, 1.
(67) Doering, D. L.; Madey, T. E. *Surf. Sci.* **1982**, *123*, 305.
(68) Kretzschmar, K.; Sass, J. K.; Hofmann, P.; Ortega, A.; Bradshaw, A. M.; Holloway, S. *Chem. Phys. Lett.* **1981**, *78*, 410.
(69) Madey, T. E.; Yates, J. J. T. *Chem. Phys. Lett.* **1977**, *51*, 77.
(70) Pache, T.; Steinruck, H. P.; Huber, W.; Menzel, D. *Surf. Sci.* **1989**, *224*, 195.
(71) Schulze, M.; Reißner, R.; Bolwin, K.; Kuch, W. *Fresenius J. Anal. Chem.* **1995**, *353*, 661.
(72) Thiel, P. A.; Hoffmann, F. M.; Weinberg, W. H. *Phys. Rev. Lett.* **1982**, *49*, 501.

believed to enhance the CO oxidation reaction by as much as 2 orders of magnitude.[15,16] Date and Haruta[15,16] suggested that water has two possible roles during CO oxidation. First, it may promote the reaction by activating molecular oxygen on the surface to enhance CO_2 production, a fact supported by related DFT calculations by Liu et al.[17] The second possible role of water is assisting in the decomposition of carbonates that may accumulate on the surface in order to accommodate additional reactants on the surface during CO oxidation. All these hypotheses propose that water promotes CO oxidation but is not directly involved in the reaction.

Here, we present evidence of oxygen exchange when water is added to an atomic oxygen-precovered Au(111) surface, resulting in oxygen scrambling on the surface as determined via temperature-programmed desorption (TPD) by employing isotopically labeled oxygen in select reactants. We also show that water is directly involved in CO oxidation on a Au(111) surface populated with atomic oxygen and water. We also investigate isotope effects on CO oxidation and water−oxygen interactions from using both $D_2{}^{16}O$ and $H_2{}^{16}O$.

Experimental Section

The experiments reported here were performed in an ultrahigh vacuum (UHV) molecular beam surface scattering apparatus that has been previously described in detail[22,73] but is briefly summarized here. The apparatus consists of a UHV scattering/analysis chamber and a quadruply differentially pumped molecular beam source chamber. The scattering/analysis chamber (base pressure less than 2.0×10^{-10} Torr) is equipped with an Auger electron spectrometer (AES), low-energy electron diffraction optics (LEED), and a quadrupole mass spectrometer (QMS).

The sample is a Au(111) single crystal (11 mm in diameter, 1.5 mm thick) mounted to a tantalum plate which can be resistively heated and which is in thermal contact with a liquid nitrogen bath for cooling. The temperature of the surface was monitored with a type-K thermocouple spot-welded to the tantalum plate. Oxygen atoms were deposited on the Au(111) surface by using a radio frequency (RF) generated plasma-jet source that produces a supersonic beam of oxygen atoms from an 8% (v) O_2 in argon gas mixture.[74–76] An oxygen dissociation fraction of ~40%, as measured by time-of-flight techniques, was achieved. Ions were deflected from the oxygen-atom beam by a charged plate (biased negatively at 3000 V) located below the beam line in one of the differential pumping stages. We have previously shown that very small surface concentrations (less than 0.02 ML) of adsorbed oxygen molecules $O_{2,a}$ are produced on the Au(111) surface from exposure to our oxygen-atom beam source; however, we reasonably neglect this species in this study because its presence is nearly undetectable.[40,41]

Research purity, isotopically labeled water (Isotec, 97.1% $H_2{}^{18}O$ and Spectra, 99.9% $D_2{}^{16}O$) was employed to distinguish the oxygen atom in water from oxygen atoms used in oxygen-atom doses [^{16}O and ^{18}O from Matheson Trigas 99.999% $^{16}O_2$ and Isotec 99.7% $^{18}O_2$, respectively). A typical value for the CO beam flux was $\sim 9 \times 10^{13}$ molecules/cm^2.

All of the beams (oxygen, water, and CO) were expanded from the same nozzle through the same apertures to ensure that the beam-illumination spots on the gold sample were the same in size and coincident. Gas lines were flushed to pressures less than 3×10^{-2} Torr before switching gases during these experiments. This pressure allows complete purging of the line after dosing gases as determined experimentally in our laboratory. In most cases, it took about 2−3 min to purge our gas lines. Purging the line after a water dose took about 10−12 min, and control experiments were performed in which we were able to determine that there was no appreciable loss of adsorbed oxygen on the gold surface during this purging time. For accuracy, we kept the same purging time between doses in all our experiments, both with and without water.

The RF generator was switched on only when it was necessary to dose atomic oxygen through the nozzle. The beam spot (~3 mm in diameter) was much smaller than the sample size to minimize the effects due to other surfaces in the chamber. When necessary, the Au(111) surface was cleaned by argon ion (1 keV, 6 μA) sputtering, followed by annealing in UHV (850 K for 10 min), a procedure which produces a carbon-free surface as verified by AES. More routine cleaning with atomic oxygen was performed after every experiment. Surface crystallinity was verified by LEED.

Oxygen coverages were estimated from the ratio of the d$N(E)$/dE peak heights, O(503 eV)/Au(239 eV) AES ratio compared to the O/Pt AES ratio of 0.3 observed for a p(2 × 2) oxygen adlayer on Pt(111), which corresponds to 3.9×10^{14} oxygen atoms/cm^2. By using a Au(239 eV)/Pt(237 eV) AES ratio of 0.95 as a conversion factor,[35] an O/Au AES ratio of 0.3 corresponds to 4.1×10^{14} oxygen atoms/cm^2 (0.29 ML). Here, 1 ML of oxygen is defined as 1.39×10^{15} atoms/cm^2 and refers to a single atomic layer of close-packed gold.

Water coverages were calculated by using a mass balance on experiments in which a CO beam impinged on a water- and atomic oxygen-precovered surface and for which CO_2, H_2O, and O_2 were all accounted. For example, when $H_2{}^{16}O$ was dosed for 6 s through the nozzle (at a pressure of 1.0 Torr) on a Au(111) surface at 77 K, the area W_1 underneath the subsequent water TPD could be integrated. The companion experiment involved precovering the Au(111) surface with 0.08 ML of ^{16}O followed by an identical 6 s $H_2{}^{16}O$ dose at 77 K and a 30 s $C^{16}O$ dose at 140 K, and the amount of CO_2 produced was recorded as A_1. A subsequent TPD showed that there was no atomic oxygen remaining on the surface, but a small amount (~25% of the initial coverage) of $H_2{}^{16}O$ was left on the surface (the area underneath this water TPD is referred to as W_2). The same CO oxidation experiment was performed without precovering the surface with $H_2{}^{16}O$, and the amount of CO_2 produced was recorded as A_2. The quantity $(A_1 - A_2)$ represents the amount of CO_2 produced by the $(W_1 - W_2)$ amount of $H_2{}^{16}O$. The value of the coverage of water represented by $(W_1 - W_2)$ can be determined by multiplying the ratio $(A_1 - A_2)/A_2$ by 0.08 ML (the oxygen-atom coverage in both experiments). This quantity can then be multiplied by the ratio $W_1/(W_1 - W_2)$ to obtain the coverage of water corresponding to the TPD area W_1 amount of $H_2{}^{16}O$. This method produced a water coverage of 0.08 ML for a 6 s water exposure (sample temperature of 77 K) with a nozzle pressure of 1.0 Torr.

DFT Calculations. Calculations of the elementary steps of CO oxidation on Au(111) were performed with DFT by using the Perdew-Wang-91 generalized gradient approximation function.[77] The core electrons of each atom were described with pseudopotentials within the projector augmented wave framework[78] as implemented in the VASP code. Kohn−Sham single-electron wave functions were expanded in a plane wave basis set up to a cutoff energy of 274 eV, appropriate for the pseudopotentials. Spin-polarized calculations were tested on each system and used when required. In our slab calculations, the Au(111) surface was modeled with four layers, in which the bottom two layers were frozen in the equilibrium bulk face-centered-cubic (fcc) lattice positions with a lattice constant of 4.173 Å, and the top two layers were relaxed. A vacuum gap of 10 Å was used to separate the periodic slabs.

(73) Wheeler, M. C.; Seets, D. C.; Mullins, C. B. *J. Chem. Phys.* **1996**, *105*, 1572.
(74) Pollard, J. E. *Rev. Sci. Instrum.* **1992**, *63*, 1771.
(75) Wheeler, M. C.; Reeves, C. T.; Seets, D. C.; Mullins, C. B. *J. Chem. Phys.* **1998**, *108*, 3057.
(76) Wheeler, M. C.; Seets, D. C.; Mullins, C. B. *J. Chem. Phys.* **1997**, *107*, 1672.
(77) Perdew, J. P. *Electronic structure of solids*; Akademie Verlag: Berlin, 1991; p 11.
(78) Kresse, G.; Joubert, D. *Phys. Rev. B* **1999**, *59*, 1758.

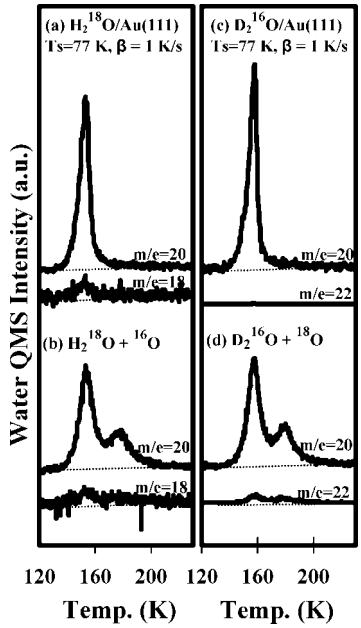

Figure 1. TPD of $H_2{}^{18}O$ ($m/e = 20$) and $H_2{}^{16}O$ ($m/e = 18$) from (a) 0.53 ML of $H_2{}^{18}O$ on clean Au(111) surface and (b) 0.53 ML of $H_2{}^{18}O$ on 0.18 ML ^{16}O-covered Au(111) surface and TPD of D_2O ($m/e = 20$) and $D_2{}^{18}O$ ($m/e = 22$) from (c) 0.53 ML of D_2O on clean Au(111) surface and (d) 0.53 ML of D_2O on 0.18 ML ^{18}O-covered Au(111) surface. All isotopically labeled water and oxygen atoms were dosed at 77 K. A heating rate of $\beta = 1$ K/s was used.

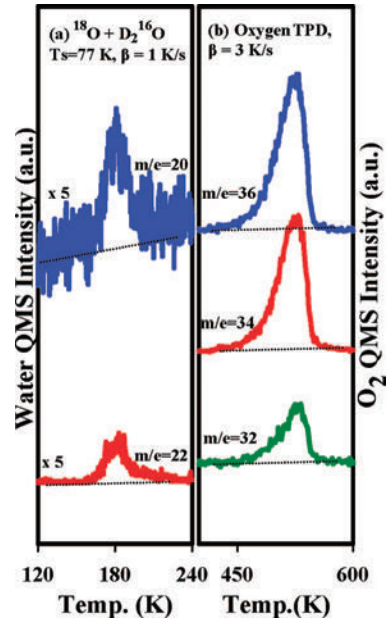

Figure 2. TPD of (a) $D_2{}^{16}O$ ($m/e = 20$) and $D_2{}^{18}O$ ($m/e = 22$) and (b) oxygen from 0.08 ML of $D_2{}^{16}O$ on 0.18 ML ^{18}O-covered surface. All isotopically labeled water and oxygen atoms were dosed at 77 K. A heating rate of $\beta = 1$ K/s was used.

Convergence with respect to the number of layers in the slab, k-point sampling, and the energy cutoff for the plane wave basis set were all checked and found to be sufficient. Coverage dependence was tested by comparing a p(2 × 2) slab with four atoms per layer and a larger p(3 × 3) slab with nine atoms per layer. A Monkhorst−Pack grid[79] of 8 × 8 × 1 for the p(2 × 2) slab and 4 × 4 × 1 for the p(3 × 3) slab was used to sample the Brillouin zone. Energy barriers and saddle points were calculated by using the climbing-image nudged elastic band[80,81] and dimer min-mode following[82,83] methods.

Results

Oxygen and Water Interaction on Au(111). Figure 1 displays TPD spectra of water ($H_2{}^{18}O$ and $D_2{}^{16}O$) from the Au(111) surface. Figure 1a shows 0.53 ML of water ($H_2{}^{18}O$, $m/e = 20$; $H_2{}^{16}O$, $m/e = 18$) desorbing from the clean Au(111) surface with a desorption peak temperature near 155 K. Water exhibits zero-order desorption kinetics from the Au(111) surface, and submonolayer and multilayer water cannot be clearly distinguished from each other.[84] The water desorption spectra from the clean Au(111) surface shown in Figure 1a are similar to spectra previously reported by Kay et al.[84] Figure 1b shows TPD spectra after exposure of 0.53 ML of $H_2{}^{18}O$ to Au(111) precovered by 0.18 ML of ^{16}O at 77 K. A new feature appears, at a higher temperature (near 175 K) than that for the clean Au(111) surface, and there is a visible decrease in intensity in the lower temperature peak. The corresponding oxygen TPD from the surface (not shown) shows mixing of the oxygen isotopes and will be discussed in detail later. Experiments similar to those in Figure 1a,b were performed by using deuterated water ($D_2{}^{16}O$) and labeled oxygen (^{18}O) adatoms. As shown in Figure 1c,d, the $D_2{}^{16}O/{}^{18}O$ results show the same general trends as the earlier results obtained by using the $H_2{}^{18}O/{}^{16}O$ combination. We observed the formation of features at comparable temperatures for $m/e = 22$ in Figure 1d, and there is a hint of this shown in Figure 1b, but the $m/e = 18$ signal is much noisier. These features are $D_2{}^{18}O$ ($m/e = 22$) which was formed as a result of oxygen exchange in the $^{18}O/D_2{}^{16}O$ system and $H_2{}^{16}O$ in the $^{16}O/H_2{}^{18}O$ system. The $m/e = 22$ feature is obviously not observed in Figure 1c in which there was no adsorbed ^{18}O on the surface prior to adding $D_2{}^{16}O$. Again, the corresponding oxygen TPD for Figure 1d shows oxygen exchange, and this will be discussed in detail immediately below.

In order to solely populate the higher temperature (175 K) water desorption peak feature, a smaller exposure (0.08 ML) of $D_2{}^{16}O$ was added to Au(111) precovered by 0.18 ML of ^{18}O at 77 K, as shown in Figure 2. Interestingly, there is no water desorption from the lower temperature peak feature (155 K) in Figure 2a, which suggests that all adsorbed water molecules are interacting strongly with adsorbed atomic oxygen. The corresponding oxygen TPD is shown in Figure 2b and will be discussed in detail later. Observations similar to those reported in Figure 2 were seen with the $H_2{}^{18}O/{}^{16}O$ system at comparable coverages. Figure 3a shows the oxygen TPD spectra from our Au(111) surface populated with 0.37 ML of ^{16}O, and Figure 3b shows the oxygen TPD spectra from our Au(111) surface populated with 0.53 ML of isotopically labeled water ($H_2{}^{18}O$) coadsorbed with 0.37 ML of ^{16}O. With the oxygen atom precoverage alone, only $^{16}O_2$ oxygen ($m/e = 32$) desorbs from the surface. However, when 0.53 ML of $H_2{}^{18}O$ was added to the ^{16}O-covered Au(111) surface, $^{16}O{}^{18}O$ ($m/e = 34$) and $^{18}O_2$ ($m/e = 36$) both desorbed from the surface in addition to mass 32. The only possible source of ^{18}O is the isotopically labeled water, $H_2{}^{18}O$. We again precovered the surface with 0.37 ML

(79) Monkhorst, H. J.; Pack, J. D. *Phys. Rev. B* **1976**, *13*, 5188.
(80) Henkelman, G.; Jonsson, H. *J. Chem. Phys.* **2000**, *113*, 9978.
(81) Henkelman, G.; Uberuaga, B. P.; Jonsson, H. *J. Chem. Phys.* **2000**, *113*, 9901.
(82) Henkelman, G.; Jonsson, H. *J. Chem. Phys.* **1999**, *111*, 7010.
(83) Olsen, R. A.; Kroes, G. J.; Henkelman, G.; Arnaldsson, A.; Jonsson, H. *J. Chem. Phys.* **2004**, *121*, 9776.
(84) Kay, B. D.; Lykke, K. R.; Creighton, J. R.; Ward, S. J. *J. Chem. Phys.* **1989**, *91*, 5120.

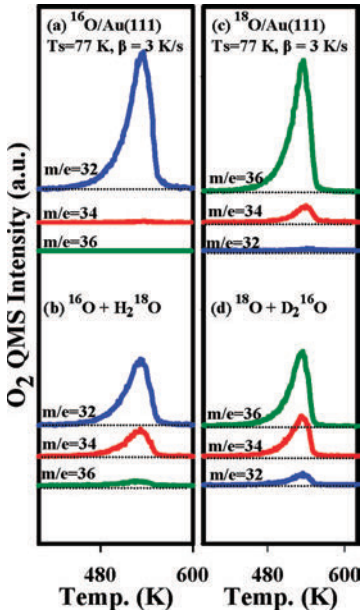

Figure 3. TPD spectra of oxygen from Au(111) after dosing (a) 0.37 ML of ^{16}O, (b) 0.53 ML of $H_2{}^{18}O$ on top of 0.37 ML of ^{16}O, (c) 0.37 ML of ^{18}O, and (d) 0.53 ML of D_2O on top of 0.37 ML of ^{18}O. All isotopically labeled water and oxygen atoms were dosed at 77 K. A heating rate of $\beta = 3$ K/s was used

of ^{18}O and performed TPD as shown in Figure 3c. As expected, the dominant desorption feature is $^{18}O_2$ ($m/e = 36$) with a small amount of $^{16}O^{18}O$ ($m/e = 34$). This mass 34 is due to some oxygen exchange in our alumina (Al_2O_3) nozzle, and it will be properly accounted for when quantitatively discussing oxygen scrambling on ^{18}O-covered surfaces. Upon adding 0.53 ML of $D_2{}^{16}O$ to a Au(111) surface precovered with 0.37 ML of ^{18}O as shown in Figure 1d, masses 36, 34, and 32 were all produced. TPD spectra (not shown) for higher oxygen coverages (as high as 1.3 ML) do not show any additional water desorption features.

Mass balance calculations were done to account for all the adsorbed water and oxygen. In the case of water, the area underneath the TPD spectra in each of the above (Figures 13) were compared with the area underneath the water TPD spectra from clean Au(111) for similar coverages. Similar mass balance calculations were done for oxygen by comparing the oxygen TPD spectra from a surface to which water was not added with the sum of the TPD areas of all oxygen-containing species (masses 32, 34, and 36) for surfaces with coadsorbed water and oxygen. We obtained agreement within 10% for all the water−oxygen experiments reported in this work.

Our DFT calculations show that a single H_2O molecule binds to the clean Au(111) surface with a binding energy of 0.15 eV, and that it is highly mobile (thus, the activation barrier for surface diffusion must be less than 0.15 eV), so that it can readily find stronger binding sites if they exist (e.g., on the oxygen-covered surface). On an oxygen-precovered surface, H_2O forms a hydrogen bond with the adsorbed oxygen adatom with an energy of 0.29 eV as shown in Figure 4, point A. From this initial state, the adsorbed atomic oxygen abstracts a hydrogen atom from the H_2O to form two hydroxyl groups on the surface. Figure 4 shows the mechanism of this reaction with a barrier of 0.11 eV (45 K activation temperature). The final state of this reaction is only 0.05 eV higher in energy than the initial state; therefore, hydroxyl formation will be very rapid and reversible between nearby H_2O and O atoms on the surface. Figure 5 shows the results of our computations regarding the

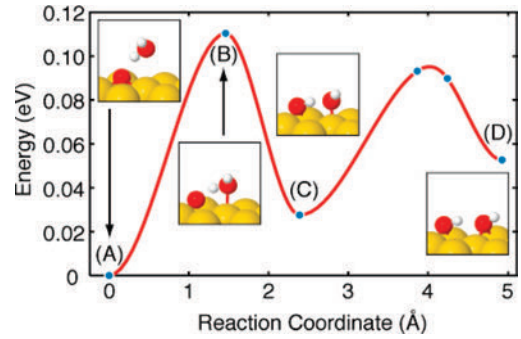

Figure 4. (A) H_2O hydrogen bonds to an oxygen atom adsorbed at the fcc site. From this initial state, a hydrogen atom can transfer (B) to the oxygen atom, forming (C) two hydroxyl groups bound in adjacent hollow sites. The low barrier and similar initial and final state energies make this reaction both fast and reversible.

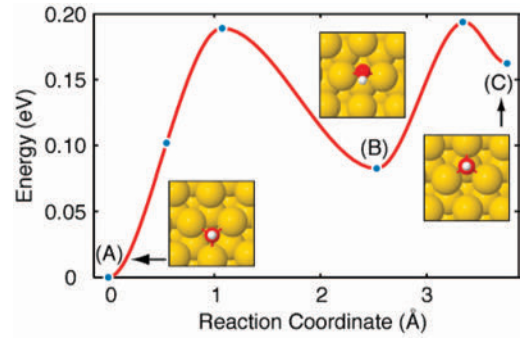

Figure 5. Hydroxyl diffuses from (A) a fcc site, (B) over a bridging transition state, and (C) into an hcp hollow. The barrier for this process is 0.19 eV.

mechanism and barrier for surface diffusion of hydroxyls on the Au(111) surface indicating rapid mobility above ∼75 K.

CO Oxidation by Coadsorbed Water and Atomic Oxygen on Au(111). We have recently studied and reported preliminary results from an investigation of low-temperature CO oxidation on Au(111) with coadsorbed water.[21] This expansion of our studies of low-temperature CO oxidation[21,22,41] by including water as a surface coadsorbate was inspired by results in which moisture enhanced low-temperature CO oxidation on metal oxide supported gold nanoclusters.[15,16]

Figure 6 demonstrates how CO reacts with oxygen originating from adsorbed water on Au(111) at 77 K. In Figure 6a, a beam of CO is impinged between 10 and 20 s on a surface precovered by 0.11 ML of ^{16}O, and as expected, only mass 44 $C^{16}O^{16}O$ is observed during the CO impingement. In Figure 6b, the CO beam is impinged on Au(111) covered only by 0.11 ML of isotopically labeled $H_2{}^{18}O$. Without preadsorbed oxygen, CO does not interact with the adsorbed water to form carbon dioxide. In Figure 6c, 0.11 ML of $H_2{}^{18}O$ is dosed on a 0.11 ML precoverage of ^{16}O on Au(111), followed by impingement of the CO beam. In this case, in addition to mass 44 $^{16}O\ C^{16}O$, which is created from CO reacting with ^{16}O on the surface, a small amount (26% of the total CO_2 produced) of mass 46 $^{16}OC^{18}O$ is observed, indicating that oxygen (in this case, ^{18}O) originating from water is directly involved in CO oxidation (no mass 48 $^{18}OC^{18}O$ is observed). A notable feature of these QMS spectra is that the CO_2 signal decays quickly (within 2−3 s), although the CO beam continues to strike the surface for 10 s. On the basis of TPD measurements following these experiments, a considerable amount of surface oxygen remains on the surface,

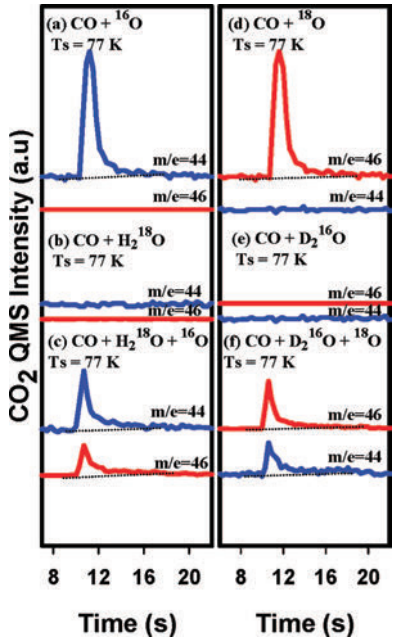

Figure 6. Evolution of CO_2 from Au(111) surface, while impinging a continuous CO beam (from 10 to 20 s.) at the surface with (a) 0.11 ML of ^{16}O atoms preadsorbed, (b) 0.11 ML of $H_2{}^{18}O$ preadsorbed, (c) 0.11 ML of $H_2{}^{18}O$ in addition to 0.11 ML of ^{16}O atoms preadsorbed, (d) 0.11 ML of ^{18}O atoms preadsorbed, (e) 0.11 ML of D_2O preadsorbed, and (f) 0.11 ML of D_2O in addition to 0.11 ML of ^{18}O atoms preadsorbed on the surface. All procedures were performed by holding the surface temperature at 77 K.

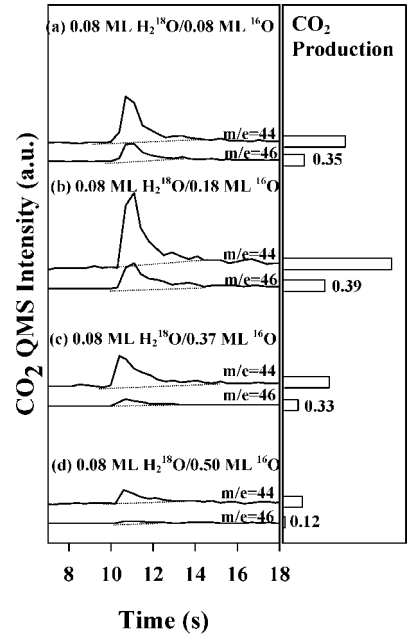

Figure 7. Evolution of CO_2 at 77 K while impinging a continuous CO beam (from 10 to 20 s.) at four different surfaces after oxygen coverages of (a) 0.08 ML, (b) 0.18 ML, (c) 0.37 ML, and (d) 0.50 ML to which 0.08 ML of $H_2{}^{18}O$ is added in each case. The bar charts on the right are relative amounts of CO_2 produced in each case as shown next to the corresponding QMS spectra. The ratio of mass 46/44 produced is shown as number labels beside each bar chart.

as well as CO. This rapid decay of CO_2 production is due to unreacted CO covering the surface, which limits further reaction at 77 K. Figure 6d−f displays similar results for CO oxidation with $D_2{}^{16}O$ and ^{18}O. As expected, only mass 46 $^{18}OC^{16}O$ is produced on the surface populated with only ^{18}O prior to the CO dose (Figure 6d), whereas there was no CO_2 produced from the surface populated with only $D_2{}^{16}O$ prior to the CO dose (Figure 6e). Figure 6f shows that, in addition to mass 46 $^{18}OC^{16}O$, mass 44 $^{16}OC^{16}O$ is produced from the surface precovered with both ^{18}O and $D_2{}^{16}O$ prior to the CO dose, indicating that adsorbed $D_2{}^{16}O$ or fragments of this molecule supplied oxygen (^{16}O) to oxidize CO to CO_2.

Figure 7 shows CO_2 evolution from gas-phase CO impinging on a Au(111) surface with coadsorbed oxygen (^{16}O) and water ($H_2{}^{18}O$) at a temperature of 77 K with various oxygen coverages. Again, the CO beam was impinged on the sample between 10 and 20 s in these experiments. Oxygen coverages were (a) 0.08 ML, (b) 0.18 ML, (c) 0.37 ML, and (d) 0.50 ML, with 0.08 ML of water in all cases. As seen in Figure 7, both mass 44 and mass 46 CO_2 were produced from impinging CO on the surface. On the right, in the bar chart, the amount of CO_2 produced is shown beside the corresponding CO_2 QMS signal. The ratios of mass 46/44 CO_2 produced are shown as labels on the bar charts for each experiment. Initially, as the ^{16}O coverage increases, the mass 44 CO_2 production increases, as more oxygen becomes available on the surface. However, as the oxygen coverage reaches higher values (higher than 0.18 ML in this case), the mass 44 CO_2 production decreases with increasing oxygen coverage. The mass 46 CO_2 production demonstrates similar behavior, where the CO_2 production peaks (at 0.18 ML oxygen coverage) and decreases as the amount of preadsorbed oxygen increases. With 0.50 ML of preadsorbed oxygen, very little mass 46 CO_2 is produced. With increasing oxygen precoverage, the ratio of mass 46/44 CO_2 decreases until it reaches 0.12 for 0.50 ML of oxygen precoverage. We initially attributed the trend in CO_2 production to site blocking as the oxygen coverage increases, limiting the availability of open adsorption sites on the surface for water and CO adsorption. In order to test our site-blocking hypothesis, we measured the initial adsorption probability of CO on surfaces identical to the ones used for the experiments shown in Figure 7. Figure 8a shows a plot of the initial CO adsorption probability as a function of varying oxygen coverages while keeping the water coverage (0.08 ML of $H_2{}^{18}O$) the same. The initial adsorption probability of CO increases with oxygen coverage at low coverages, peaks at 0.50 ML, and decreases with further increase in coverage. In Figure 8b, 0.37 ML of ^{16}O was used in all cases while varying the $H_2{}^{18}O$ coverages. The CO adsorption probability again increases with $H_2{}^{18}O$ coverage, peaks at 0.13 ML of $H_2{}^{18}O$ coverage, and subsequently decreases. Points 1, 2, and 3 in Figure 8 show a comparison of CO adsorption on clean Au(111), oxygen-covered Au(111) (0.18 ML of ^{16}O) without water, and a surface covered with both oxygen (0.18 ML) and water (0.08 ML). We observed that the initial sticking probability was greatly enhanced compared to that of the clean surface by precovering the surface with solely oxygen (74% increase) and even more so by precovering with both oxygen and water (94% increase) in the low-coverage regime. It appears from the initial adsorption probability measurement that the observed CO oxidation trends reported in Figure 7 are not due to site blocking. A possible explanation for the change in reactivity at higher oxygen coverages is the formation of 3D oxygen clusters as earlier reported by Min et al.[32] Additionally, we have measured reductions in the reactivity of oxygen overlayers on Au(111) after annealing.[85]

In order to further explore the direct involvement of water in CO_2 production, we compared the total amount of CO_2 produced

(85) Ojifinni, R. A.; Gong, J. L.; Kim, T. S.; Mullins, C. B. In preparation.

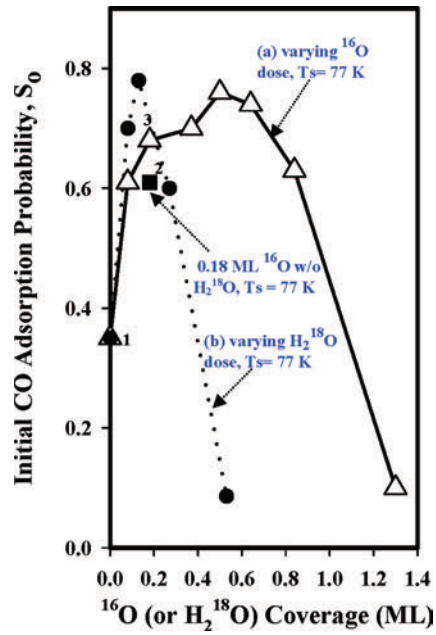

Figure 8. Initial CO adsorption probability (S_o) at 77 K by using the method of King and Wells. A CO pulse of 2.0 s was dosed on Au(111) with varying ^{16}O coverages (0.08, 0.18, 0.37, 0.5, 0.64, and 0.84 ML) followed by 0.08 ML of $H_2{}^{18}O$ dose in each case (triangles) and 0.37 ML of ^{16}O to which varying $H_2{}^{18}O$ coverages (0.08, 0.13, 0.27, and 0.53 ML) were added (solid circles). Data points labeled 1, 2, and 3 represent S_o values measured on clean Au(111) (1), Au(111) covered with 0.18 ML of ^{16}O (2), and 0.18 ML of ^{16}O with 0.08 ML $H_2{}^{18}O$ added prior to CO dose (3).

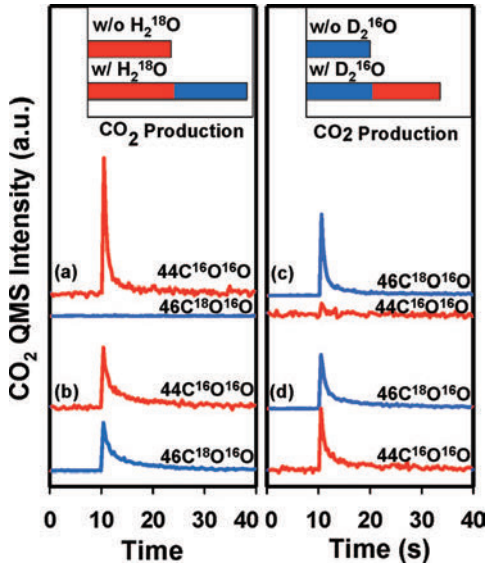

Figure 9. Evolution of CO_2 at 140 K while impinging a continuous CO beam (from 10 to 40 s.) at the surface. (a) 0.11 ML of ^{16}O preadsorbed without $H_2{}^{18}O$, (b) 0.14 ML $H_2{}^{18}O$ in addition to 0.11 ML of ^{16}O atoms preadsorbed on Au(111) at 77 K, (c) 0.11 ML of ^{18}O preadsorbed without D_2O, and (d) 0.14 ML of D_2O in addition to 0.11 ML of ^{18}O atoms preadsorbed at 77 K. The area underneath the plots between 10 and 40 s represents the amount of CO_2 produced as shown in the insets.

from a solely oxygen-covered Au(111) surface with that of a Au(111) surface covered with both atomic oxygen and water. These experiments (shown in Figure 9) were performed at 140 K to prevent accumulation of adsorbed CO. This temperature is well below the maximum desorption peak temperature (175 K) for water on oxygen-covered Au(111) but above the desorption peak temperature (108 K) for CO. This kept the surface coverage of CO very low by reducing the residence time of CO on the surface. Although the data are not shown here, we note that adsorbed water alone will not oxidize CO at 140 K, just as for a surface temperature of 77 K as shown in Figure 6b.

In Figure 9a, a CO beam is impinged on 0.11 ML of ^{16}O at 140 K. The area underneath the curve between 10 and 40 s represents the amount of mass 44 CO_2 produced, as shown in the inset. As expected, no mass 46 CO_2 is detected in this case. In Figure 9b, both masses 44 CO_2 and 46 CO_2 were produced when a CO beam was impinged on the surface covered by 0.11 ML of ^{16}O and 0.14 ML of $H_2{}^{18}O$. The inset shows the total amount of CO_2 produced for each case in a bar chart, with the red bar representing mass 44 CO_2 and the blue bar representing mass 46 CO_2. Much more CO_2 (91% more in Figure 9b than in Figure 9a) is produced when water is added to the oxygen layer on the surface prior to CO impingement. TPD experiments (not shown) following the experiment in Figure 9b showed that ~0.04 ML of the initially adsorbed $H_2{}^{18}O$ is left unreacted on the surface. Similar results are obtained with the Au(111) surface precovered by 0.11 ML of ^{18}O and 0.14 ML of $D_2{}^{16}O$ as shown in Figure 9c,d.

Isotope Effects on Water−Oxygen Interactions and Water-Enhanced CO Oxidation. We investigated isotope effects in water−oxygen interactions by using atomic oxygen (^{18}O) with both water ($H_2{}^{16}O$) and deuterated water ($D_2{}^{16}O$). Figure 10a shows water TPD spectra from a 0.18 ML ^{18}O-precovered Au(111) surface to which 0.27 ML of $H_2{}^{16}O$ was added at 77 K, and Figure 10c shows the corresponding oxygen TPD spectra from this surface. Both $H_2{}^{16}O$ (m/e = 18) and $H_2{}^{18}O$ (m/e = 20) are produced as seen in Figure 10a. A total of 0.18 ML of ^{18}O was again dosed on Au(111) at 77 K. This step was followed by the addition of 0.27 ML of $D_2{}^{16}O$ with subsequent TPD producing both $D_2{}^{16}O$ (m/e = 20) and $D_2{}^{18}O$ (m/e = 22) as shown in Figure 10b. Figure 10d shows the corresponding oxygen TPD spectra for this $^{18}O/D_2{}^{16}O$ case. In order to make a comparison between $H_2{}^{16}O$ and $D_2{}^{16}O$, we used water coverages that were within 6% of each other as determined by TPD, and the oxygen dose experiments were in agreement to within 1%. Quantitative analysis of the TPD data in Figure 10 shows that $H_2{}^{18}O$ (m/e = 20) accounted for 36% of the total amount of water produced in the $^{18}O/H_2{}^{16}O$ case, compared to only 6% $D_2{}^{18}O$ (m/e = 22) in the $^{18}O/D_2{}^{16}O$ case. Another measure of this isotope effect is the relative amount of unscrambled $^{18}O_2$ (m/e = 36) compared to the total amount of molecular oxygen evolving from the surface from the water−oxygen interaction. The $^{18}O/H_2{}^{16}O$ case had 16% unscrambled mass 36, with most of the initial ^{18}O ending up in $H_2{}^{18}O$. However, in the $^{18}O/D_2{}^{16}O$ case, 31% unscrambled mass 36 was produced as less of the initial ^{18}O ended up in $D_2{}^{18}O$.

To investigate isotope effects in CO oxidation, three complementary CO oxidation experiments were performed. The first experiment is a precoverage of 0.08 ML of ^{16}O on Au(111) at 77 K (without any preadsorbed water) followed by CO impingement for 30 s. The second experiment involves the addition of 0.08 ML of $H_2{}^{16}O$ to a 0.08 ML ^{16}O-covered surface at 77 K, followed by CO impingement for 30 s at 140 K. In the third experiment, 0.08 ML of $D_2{}^{16}O$ was added to a 0.08 ML ^{16}O-covered surface at 77 K prior to a 30 s CO dose at 140 K, as shown in Figure 11. We determined the amount of CO_2 produced in each case by integrating the area underneath the corresponding CO_2 QMS signal and observed that the surface with coadsorbed $H_2{}^{16}O$ produced 24% more CO_2 than the surface with coadsorbed $D_2{}^{16}O$. Additionally, subsequent water TPD spectra showed that 75% of the adsorbed $H_2{}^{16}O$ reacted

on the surface, whereas only 38% reacted in the case of $D_2{}^{16}O$. This could be anticipated because the experiments shown earlier in Figure 10 showed that less $D_2{}^{16}O$ (compared to $H_2{}^{16}O$) reacts with the adsorbed oxygen overlayer, thus making fewer adsorbed hydroxyl groups with which impinging CO can react. Comparing both cases in which water was added, we see that more CO_2 is produced than in the case where the surface is without water. Figure 11 shows that 70% more CO_2 (compared with the surface without water added) is produced when $H_2{}^{16}O$ is added and 27% more CO_2 (compared with the surface without water added) is produced when $D_2{}^{16}O$ is added.

Discussion

In the previous section, we presented experimental results pertaining to water strongly reacting with adsorbed atomic oxygen to produce OH groups as well as water (or OH) directly reacting with CO to produce CO_2 on the Au(111) surface. We observed an upward shift in the water desorption temperature and oxygen scrambling when atomic oxygen and water were coadsorbed on the surface. The direct involvement of water was observed in CO oxidation by the production of $^{16}OC^{18}O$ (in addition to $^{16}OC^{16}O$) during CO impingement on a surface covered by both $H_2{}^{18}O$ and ^{16}O. We therefore present the following to further elucidate the foregoing results:

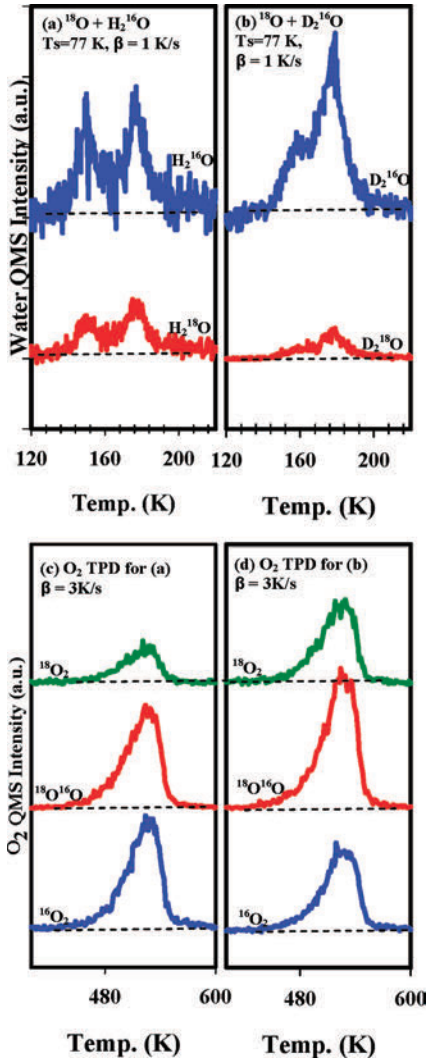

Figure 10. (a) TPD of $H_2{}^{16}O$ (m/e = 18) and $H_2{}^{18}O$ (m/e = 20) from 0.27 ML of $H_2{}^{16}O$ on 0.18 ML ^{18}O-covered Au(111) surface. (b) TPD of $D_2{}^{16}O$ (m/e = 20) and $D_2{}^{18}O$ (m/e = 22) from 0.27 ML of $D_2{}^{16}O$ on 0.18 ML ^{18}O-covered Au(111) surface. (c) and (d) are the oxygen TPD spectra corresponding to panels a and b, respectively. All isotopically labeled water and oxygen atoms were dosed at 77 K. A heating rate of β = 1 K/s was used for water and 3 K/s for oxygen.

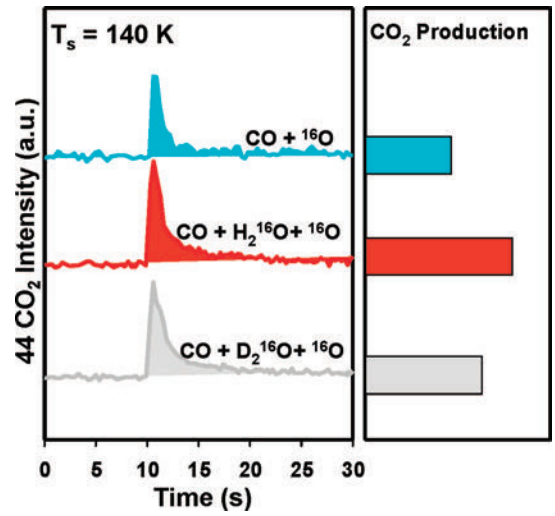

Figure 11. Mass 44 CO_2 evolution at 140 K while impinging a continuous CO beam (from 10 to 40 s.) on a Au(111) with (a) 0.08 ML of ^{16}O atoms preadsorbed at 77 K without $H_2{}^{16}O$, (b) 0.08 ML of $H_2{}^{16}O$ added in addition to 0.08 ML of ^{16}O, and (c) 0.08 ML of $D_2{}^{16}O$ added in addition to 0.08 ML of ^{16}O. The bar charts on the right are relative amounts of CO_2 produced in each case as shown next to the corresponding QMS spectra.

1. Water Interaction with Adsorbed Atomic Oxygen. Water interacts with adsorbed atomic oxygen to form either hydroxyls or a water−oxygen complex, and water−oxygen interactions produce oxygen exchange between water and adsorbed oxygen. The formation of stable H_2O-O complexes on the surface results in an upward shift in the water desorption peak temperature (Figure 1b) compared to water desorption from the pristine single-crystal metal surface (Figure 1a). As alluded previously, for the Au(111) surface, the metal−water interaction is comparable to the water−water interaction, and there is no distinct monolayer water TPD feature.[84] In contrast, with the oxygen precovered surface, one can imagine water forming hydrogen bonds with the oxygen adlayer and binding more strongly than on the clean Au(111) surface. This observation was supported by results from our DFT calculations, in which hydroxyl formation is favorable even at 45 K because of the low activation energy (0.11 eV), as seen in Figure 4. This higher desorption temperature feature was also observed by Lazaga et al.[25] on the oxygen-precovered Au(111) surface, and it was attributed to oxygen-stabilized water or recombination and disproportionation of OH groups. They proposed that during the TPD of this surface, the H_2O-O complex decomposes to evolve water, thereby leaving the original oxygen atom on the surface.[25]

The absence of the lower-temperature feature (near 155 K) with 0.08 ML of $D_2{}^{16}O$ coverage in addition to 0.18 ML of ^{18}O coverage as shown in Figure 2a indicates that all adsorbed water molecules are interacting with adsorbed atomic oxygen. Similar observations (not shown) were seen with the $H_2{}^{18}O/{}^{16}O$ system at similar coverages. We propose here that all the water molecules readily formed hydroxyls upon interacting with the oxygen overlayer on the Au(111) surface. However, we observed $H_2{}^{16}O$ (m/e = 18 in Figure 1b from coadsorbed ^{16}O and $H_2{}^{18}O$) and $D_2{}^{18}O$ (m/e = 22 in Figure 1d from coadsorbed ^{18}O and $D_2{}^{16}O$), both from the low-temperature water desorption

peak (155 K), an observation that might be explained, as mentioned earlier, by the rapid diffusion of OH groups above 75 K as determined by our DFT calculations (Figure 5).

A strong water−oxygen interaction resulting in oxygen scrambling between water and adsorbed oxygen atoms is shown in Figure 3a,b. We attribute this to OH recombination after oxygen had activated water or perhaps abstracted hydrogen from water to create OH groups. Upon heating, OH groups recombine to form water, leaving an oxygen atom on the surface. In the process, oxygen scrambling occurs just as on many other metal surfaces. We note that with only water on Au(111) (i.e., no preadsorbed oxygen), there was no indication of water dissociation or recombinative oxygen desorption near 535 K. This molecular adsorption of water without dissociation on clean Au(111) has also been previously reported in XPS and TPD experiments.[25] Outka and co-workers also observed isotope mixing when they coadsorbed ^{18}O and $H_2{}^{16}O$ on Au(110) during TPD measurements[35] and also ascribed this oxygen scrambling to either decomposition of oxygen-stabilized water or disproportionation of surface hydroxyls. They suggest that the Brønsted-base character of oxygen adatoms is sufficient to abstract an acidic hydrogen atom from the adsorbed water molecule on the group 1B metals.[35]

The presence of $^{16}O^{18}O$ in all the oxygen TPD spectra following water and oxygen ($^{16}O/H_2{}^{18}O$ and $^{18}O/D_2{}^{16}O$) exposures on Au(111) surface clearly demonstrates that the water is reacting with the oxygen overlayer. In this surface reaction, oxygen atoms in the original precoverage preparation get scrambled with oxygen atoms that originate in water ending up as surface atoms on Au(111), and vice-versa, subsequently desorbing to produce $^{16}O^{18}O$. Corresponding DFT calculations indicate that there is rapid diffusion of hydroxyls at temperatures as low as 75 K (Figure 5), which helps explain the facile oxygen exchange between water and adsorbed oxygen atoms observed in both water desorption peaks and in the oxygen desorption.

2. Water-Enhanced CO Oxidation. Water directly enhances CO oxidation on the oxygen-precovered Au(111) surface to produce more CO_2 than without water. As stated in the Results section, our experiments involving CO oxidation on an atomic oxygen (^{16}O) and water ($H_2{}^{18}O$) coadsorbed Au(111) surface produced both $C^{16}O_2$ and $^{18}OC^{16}O$ (the same for the case of $^{18}O/D_2{}^{16}O$) as seen in Figure 6. We propose that this is due to CO reacting with either activated water or hydroxyls on the surface. Although we cannot confirm the exact nature of the activated water on the surface, we note that formation of hydroxyl groups by adding water to an oxygen overlayer on a transition-metal surface at low temperature is not uncommon. Sueyoshi et al. have shown with HREELS on Cu(100) that oxygen atoms can abstract hydrogen from water to form hydroxyls at temperatures as low as 100 K,[86] and similar reactions may take place on Au(111). We also noted that by impinging CO directly on a Au(111) surface covered with only water, there was no CO_2 produced, further supporting the notion that water does not dissociate on clean Au(111).[25]

To further investigate water-enhanced CO oxidation, we carried out DFT calculations on reactions involving CO, O, and H_2O on the Au(111) surface. We find that there are three distinct possible reaction pathways resulting in the formation of CO_2. The CO oxidation mechanism is similar for each pathway, but they differ in regards to if and when a hydrogen atom is abstracted from the H_2O molecule by the adsorbed oxygen atom as it oxidizes CO.

(86) Sueyoshi, T.; Sasaki, T.; Iwasawa, Y. *J. Phys. Chem. B* **1997**, *101*, 4648.

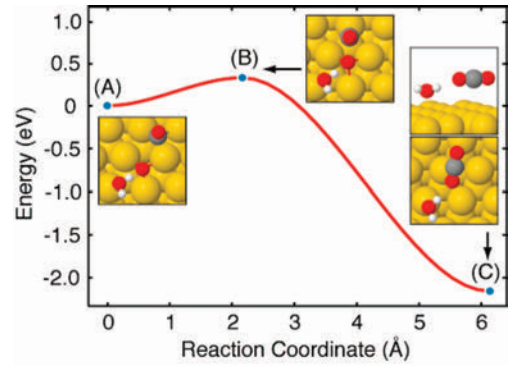

Figure 12. H_2O acting as a spectator in the CO oxidation reaction (A−C). The barrier of 0.33 eV is higher than that for the reaction without water molecules present.

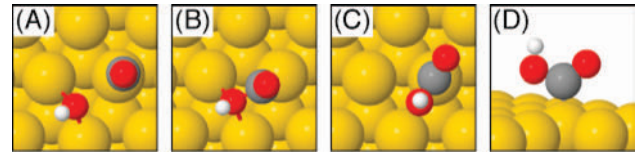

Figure 13. Formation of OCOH from the reaction of CO with OH. The barrier for this reaction is 0.32 eV.

In reaction pathway I, adsorbed oxygen adatoms are hydrogen-bonded to H_2O (a spectator molecule) as they react with CO. The mechanism of this reaction, which has a barrier of 0.33 eV, is depicted in Figure 12. This process is very similar to the oxidation of CO by an oxygen adatom which has a somewhat lower barrier of 0.25 eV. With H_2O present, the initial state is stabilized, and the reaction barrier is increased. This pathway is consistent with the prompt but slower (than that without adsorbed water) reaction of water and oxygen with CO at temperatures as low as 77 K. However, this pathway does not allow for more CO_2 to be produced, as is observed experimentally.

In reaction pathway II, we allow adsorbed OH to be formed prior to CO oxidation (pathway II is different from pathway I, in which there was no OH formation). From the calculation displayed in Figure 4, we know that adsorbed H_2O will react with a chemisorbed oxygen atom, donating a hydrogen atom to form two adsorbed hydroxyl groups. The barrier for this reaction is low (0.11 eV) so that when H_2O is deposited on an oxygen-precovered surface, adsorbed OH species are expected to form (which is consistent with our experimental observations). Once surface OH groups are formed, they can subsequently react with CO as shown in Figure 13. Formation of a carboxylate (OCOH) intermediate occurs spontaneously when CO and isolated OH meet. The OCOH molecule is firmly bound to the surface with an energy of 1.84 eV. In order for CO_2 to form, the hydrogen atom must be transferred to the surface or to another molecule on the surface. We considered the following two possibilities:

1. The OCOH molecule undergoes a cis−trans isomerism (Figure 14A−C), and then, the hydrogen atom is abstracted by the gold surface (Figure 14D−F). Both processes have high barriers (0.44 and 0.93 eV, respectively).
2. The OCOH molecule transfers the hydrogen to an existing molecule on the surface. We considered a hydroxyl acceptor as shown in Figure 15. The OH molecule near the OCOH is shown in Figure 15, point A. The hydrogen transfer to OH, Figure 15, point B, has a much lower

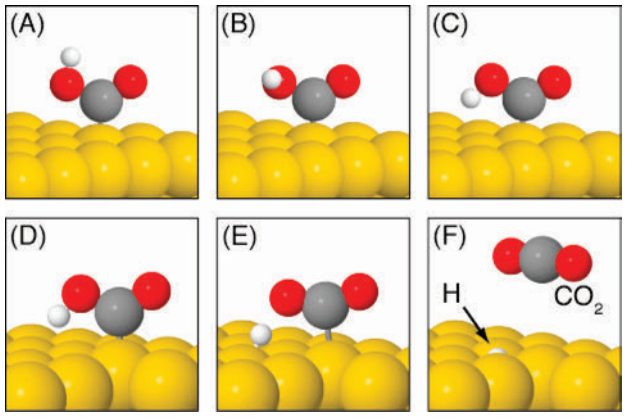

Figure 14. When OCOH forms from the reaction of CO with OH, the hydrogen is positioned away from the surface (A). In order to form CO_2, the molecule must first undergo a conformational change (B−C), with a barrier of 0.44 eV, so that the hydrogen atom can then transfer to the surface (D−F). The hydrogen transfer process occurs with a prohibitively high barrier of 0.93 eV.

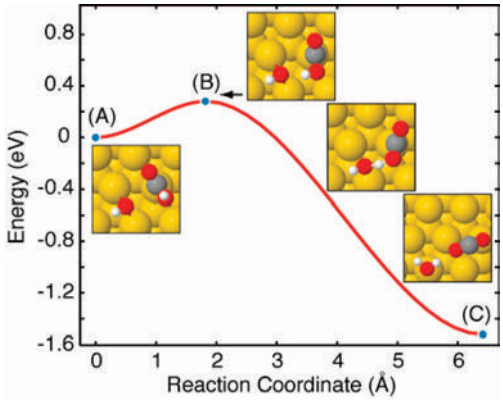

Figure 15. Hydrogen transfer from OCOH to OH (A), over a barrier of 0.28 eV (B), to form H_2O and CO_2 (C).

barrier (0.28 eV) than that for hydrogen transfer to the surface (0.93 eV), because the transfer distance is reduced and the products (H_2O and CO_2) are lower in energy (Figure 15, point C).

Pathway III starts the same way as pathway II, with hydrogen transfer between a H_2O molecule and an oxygen adatom. The resulting two OH adspecies are held together by a hydrogen bond; therefore, they are unlikely to diffuse away from each other at low temperature. Then, if a CO molecule diffuses to one of the OH molecules, a concerted hydrogen-transfer CO oxidation reaction occurs as seen in Figure 16. The barrier for the reaction, 0.11 eV, is actually due to CO diffusion. As CO meets one of the OH adspecies, a long OCOHOH intermediate geometry is formed (Figure 16, point C). Here, the middle OH dissociates to simultaneously form H_2O and CO_2. Another way of describing this reaction is that CO oxidation with OH takes place to form CO_2 as the hydrogen from the OH transfers to a neighboring OH to form H_2O. However, this pathway cannot exclusively account for all the chemistry taking place on the surface because this mechanism is inconsistent with more CO_2 being produced with the addition of water, as is observed experimentally.

The energy landscape for the above three pathways is shown in Figure 17. Each process has the same initial state, with O, H_2O, and CO adsorbed on Au(111) in that order. The zero of energy is a clean surface and CO, ½O_2, and H_2O in the gas phase. In both pathways I and II, the molecules get trapped in

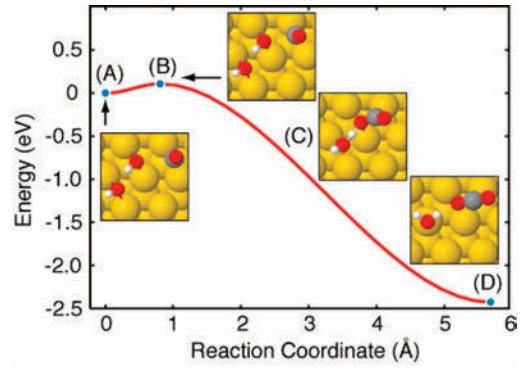

Figure 16. (A) Initial state configuration (after H_2O dissociation) with two OH groups bound to the surface. (B) The transition state of the reaction is due to the 0.11 eV diffusion barrier of CO. (C) Intermediate configuration in which the hydrogen in one hydroxyl is spontaneously transferred to the other hydroxyl to form H_2O and CO_2. (D) The final transition state of the reaction with H_2O is bound to the surface, and CO_2 has desorbed.

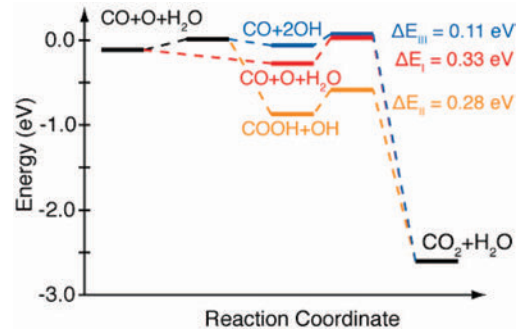

Figure 17. Energy landscape for three reaction mechanisms of CO oxidation in the presence of H_2O. In pathway I (red), there is no hydrogen transfer from H_2O. In pathway II (orange), hydrogen transfer occurs before CO oxidation. In pathway III (blue), hydrogen transfer occurs concertedly with CO oxidation, leading to the lowest overall barrier for CO oxidation (0.11 eV).

intermediate minima from which barriers of 0.33 eV and 0.28 eV, respectively, must be overcome to form CO_2. In pathway III, no such low-energy intermediate is formed, and the overall CO oxidation reaction has a barrier of 0.11 eV and can occur at temperatures as low as 45 K. This is consistent with our experimental observation in which CO oxidation in the presence of water readily occurs at $T_s = 77$ K. It is also worthwhile to state here that our observed experimental results are likely occurring because of a combination of two or more of the above reaction pathways described by DFT calculations.

It may be useful to compare the chemistry reported here with the water−gas shift reaction (WGS). The WGS is a reversible, exothermic reaction of carbon monoxide and water. Two possible mechanisms have been proposed for this reaction.[87] The first mechanism is the associative mechanism,[88–90] with the following reaction steps:

$$CO_{gas} \rightarrow CO_{ads} \quad (1)$$

$$H_2O_{gas} \rightarrow H_2O_{ads} \quad (2)$$

$$H_2O_{ads} \rightarrow OH_{ads} + H_{ads} \quad (3)$$

(87) Gorte, R. J.; Zhao, S. *Catal. Today* **2005**, *104*, 18.
(88) Grenoble, D. C.; Estadt, M. M.; Ollis, D. F. *J. Catal.* **1981**, *67*, 90.
(89) Salmi, T.; Hakkarainen, R. *Appl. Catal.* **1989**, *49*, 285.
(90) Vanherwijnen, T.; Dejong, W. A. *J. Catal.* **1980**, *63*, 83.

$$CO_{ads} + OH_{ads} \rightarrow HCOO_{ads} \quad (4)$$

$$HCOO_{ads} \rightarrow CO_{2,gas} + H_{ads} \quad (5)$$

$$2H_{ads} \rightarrow H_{2,gas} \quad (6)$$

The process indicates that the hydroxyl group from water dissociation combines with CO to form a formate intermediate, which then decomposes into CO_2 and hydrogen. Formate dissociation is regarded as the rate-determining step in the associative mechanism of the WGS reaction. The second mechanism is the redox mechanism,[91,92] in which CO directly reacts with adsorbed oxygen to form CO_2 following the complete dissociation of water into atomic oxygen and molecular hydrogen as follows:

$$CO_{gas} \rightarrow CO_{ads} \quad (1)$$

$$H_2O_{gas} \rightarrow H_2O_{ads} \quad (2)$$

$$H_2O_{ads} \rightarrow H_{2,gas} + O_{ads} \quad (3)$$

$$CO_{ads} + O_{ads} \rightarrow CO_{2ads} \quad (4)$$

$$CO_{2,gas} \rightarrow CO_{2,gas} \quad (5)$$

A recent study[93] has reported the high performance of TiO_2-x/Au(111) and CeO_2-x/Au(111) catalysts in the WGS reaction. This study claims that although clean Au(111) is not catalytically active for the WGS, Au(111) surfaces that are 20−30% covered by ceria or titania NPS have activities comparable to those of good WGS catalysts such as Cu(111) or Cu(100).[93] The reaction is said to occur by water dissociating on oxygen vacancies of the oxide NPS while CO adsorbs on Au sites located nearby, and subsequent reaction steps take place at the metal−oxide interface.[93] The following was proposed[93] as the reaction mechanism based on DFT calculations:

$$CO_{gas} \rightarrow CO_{ads} \quad (1)$$

$$H_2O_{gas} \rightarrow H_2O_{ads} \quad (2)$$

$$H_2O_{ads} \rightarrow OH_{ads} + H_{ads} \quad (3)$$

$$CO_{ads} + OH_{ads} \rightarrow HOCO_{ads} \quad (4)$$

$$HOCO_{ads} \rightarrow CO_{2,gas} + H_{ads} \quad (5)$$

$$2H_{ads} \rightarrow H_{2,gas} \quad (6)$$

Erdohelyi and co-workers' infrared (IR) spectroscopy study of the reaction of CO with water over catalysts composed of iridium supported on oxides (MgO, Al_2O_3, SiO_2, and TiO_2) revealed that formate is the reaction intermediate, which is in agreement with the associative mechanism above.[94] Formate ions were observed as new IR bands at 1590 and 1380 cm^{-1} (at 473 K) and were assigned to the asymmetric and symmetric O−C−O stretching vibrations of the absorbed formate ion.[94] A recent DFT calculation of CO reaction with water on $Pt_2Mo(111)$ showed that water dissociation into H_{ads} and OH_{ads} was followed by CO reaction with the hydroxyl to form COOH, which later decomposes to CO_2 and H_{ads} in the forward reaction or CO and OH_{ads} in the reverse reaction.[95] The associative mechanism with a COOH intermediate is a plausible reaction on Au(111) as well, with the only difference being reaction step 2, where atomic oxygen abstracts a hydrogen from water to form surface hydroxyls. The redox mechanism is very unlikely on Au(111) because it is not known to completely dissociate water to hydrogen and oxygen.[66]

The reaction of CO and OH to form CO_2 is widely studied in gas-phase chemistry because of the pivotal role of OH radicals in atmospheric chemistry.[96,97] Many other investigations of CO and OH reactions on metal surfaces are motivated by electrochemistry.[98–100]One relevant study regarding the reaction of adsorbed CO and OH on Pt(111) under UHV conditions performed by Bergeld et al.[98] showed that water can promote CO oxidation on oxygen-covered Pt(111). They observed that a new CO_2 desorption feature near 200 K appears when water is coadsorbed prior to temperature-programmed reaction of a Pt(111) surface populated with CO and atomic oxygen. This new peak occurs at a much lower temperature than does the CO_2 desorption peak (~300 K) for a typical surface reaction between CO and oxygen adatoms on Pt(111), and it has been attributed to CO reacting with OH groups on the surface. A similar reaction may occur on Au(111), in which hydroxyls are formed from water splitting and reacting with CO to form CO_2 at 77 K. Related calculations performed by Gong et al. demonstrated that on Pt(111), CO_2 formation is likely to follow a mechanism in which CO first reacts with OH to form surface COOH, followed by this COOH reacting with OH to form CO_2 and H_2O.[101]

Our observation that much more CO_2 is produced when water is added to the oxygen layer on the surface (insets in Figure 9) is similar to what Bergeld et al. observed on Pt(111), where they demonstrated the promotional effect of water on CO oxidation.[98] On the basis of our TPD measurements after CO impingement at 140 K (not shown here), no detectable amount of oxygen remained on the surface. However, a small amount (~0.04 ML) of the initial $H_2{}^{18}O$ was observed during the reaction. CO oxidation on a surface covered with ^{18}O and $D_2{}^{16}O$ showed similar observations (Figure 9c,d), and again, we speculate that activated water or OD from $D_2{}^{16}O$ is responsible for CO oxidation. We might expect a difference in the rate of CO_2 production because of a kinetic isotope effect on CO oxidation as a result of the OH versus OD bond, and this is discussed later in this paper. As mentioned earlier, the total amount of CO_2 produced when water is added to the oxygen-precovered surface increases. This is a clear indication that water contributes some additional oxygen for CO oxidation and that water does not simply exchange oxygen atoms with adsorbed oxygen on the surface. A simple oxygen exchange would result in the same CO_2 production on both surfaces (i.e., with and without water) because there would be the same amount of adsorbed oxygen atoms.

It is also possible to argue that this additional CO_2 is produced from additional oxygen atoms created by complete dissociation of water on the oxygen-covered surface. In this case, water may lose a hydrogen atom to a nearby oxygen atom, and the resulting OH groups further dissociate on the surface to leave oxygen atoms on

(91) Bunluesin, T.; Gorte, R. J.; Graham, G. W. *Appl. Catal., B* **1998**, *15*, 107.
(92) Chinchen, G. C.; Spencer, M. S. *J. Catal.* **1988**, *112*, 325.
(93) Rodriguez, J. A.; Ma, S.; Liu, P.; Hrbek, J.; Evans, J.; Perez, M. *Science* **2007**, *318*, 1757.
(94) Erdohelyi, A.; Fodor, K.; Suru, G. *App. Catal., A* **1996**, *139*, 131.
(95) Wang, J. G.; Hammer, B. *J. Catal.* **2006**, *243*, 192.
(96) Lester, M. I.; Pond, B. V.; Anderson, D. T.; Harding, L. B.; Wagner, A. F. *J. Chem. Phys.* **2000**, *113*, 9889.
(97) Rockmann, T.; Brenninkmeijer, C. A. M.; Saueressig, G.; Bergamaschi, P.; Crowley, J. N.; Fischer, H.; Crutzen, P. J. *Science* **1998**, *281*, 544.
(98) Bergeld, J.; Kasemo, B.; Chakarov, D. V. *Surf. Sci.* **2001**, *495*, L815.
(99) Hayden, B. E.; Rendall, M. E.; South, O. *J. Am. Chem. Soc.* **2003**, *125*, 7738.
(100) Lei, T.; Zei, M. S.; Ertl, G. *Surf. Sci.* **2005**, *581*, 142.
(101) Gong, X. Q.; Hu, P.; Raval, R. *J. Chem. Phys.* **2003**, *119*, 6324.

the surface. However, it is well-known that on metals that do not dissociate water on their clean surfaces (this group includes the Au(111) surface), OH dissociation is not favored over two OH groups recombining to form one water, leaving an oxygen atom on the surface.[66] Consequently we rule out the likelihood of additional oxygen on the surface because of complete dissociation of water as being responsible for the additional CO_2 produced on the surface. This is consistent with our DFT calculations showing that the dissociation of OH on Au(111) is endothermic by 1.33 eV and hence not activated below room temperature. However, in our attempts to account for all the adsorbed species, we did not detect molecular hydrogen or hydrogen-containing species, such as H_2CO and HCOOH, during CO impingement reaction or subsequent TPD measurements. A residual-gas analysis during one of the experiments did not show molecular hydrogen or any other hydrogen-containing species different from those in the UHV background. Previous works[15,16,98] have also reported that no molecular hydrogen was detected in water-assisted CO oxidation reactions. We speculate that hydrogen atoms released on the surface during reaction recombine and desorb at a rate that is undetectable.

3. Kinetic Isotope Effects. Differences in reactivity of $H_2{}^{16}O$ and $D_2{}^{16}O$ with oxygen (^{18}O) and the relative CO_2 production with H_2O and $D_2{}^{16}O$ are indicative of kinetic isotope effects. The observed decrease in oxygen scrambling in the $^{18}O/D_2{}^{16}O$ system compared to the $^{18}O/H_2{}^{16}O$ system (Figure 10) is likely due to a kinetic isotope effect in water−oxygen interactions during the formation of hydroxyls or a water−oxygen complex. Formation of $H_2{}^{18}O$ will be favored over $D_2{}^{18}O$ under identical reaction conditions because the O−H bond is weaker than the O−D bond because of zero-point energy differences. There was a higher degree of oxygen scrambling when ^{18}O and $H_2{}^{16}O$ were coadsorbed on the surface with only 16% of the total $^{18}O_2$ remaining unscrambled, compared to 31% unscrambled $^{18}O_2$ when ^{18}O and $D_2{}^{16}O$ were coadsorbed on the surface.

The fact that CO oxidation on the surface with the $^{16}O/H_2O$ ad-mixture produced ~24% more CO_2 than the one with the $^{16}O/D_2{}^{16}O$ ad-mixture also suggests kinetic isotope effects in water-enhanced CO_2 production as shown in Figure 11. As mentioned earlier, the surface with OH groups produced 70% more CO_2 than the surface without any water, whereas the surface with OD groups produced only 27% more CO_2 than the surface without any water added, also shown in Figure 11. However, it is likely that there are fewer OD species on the surface than OH species on the basis of the observation that 75% of the initial H_2O coverage reacted on the $^{16}O/H_2O$ surface, whereas only 38% of the initial $D_2{}^{16}O$ reacted in the case of the $^{16}O/D_2{}^{16}O$ ad-mixture, as seen from water TPD data (not shown) following the experiments in Figure 11. Thus, it is difficult to construct a consistent experiment which would allow the CO reactivity of adsorbed OH to be compared with that of OD.

Kinetic isotope effects were observed by Wieckowski[102] between H_2O and D_2O in HCOOH and CH_3OH adsorption and oxidation on platinum electrodes in a sulfuric acid electrolyte. This study attributed the observed kinetic isotope effects in the oxidation of methanol and formic acid to adsorbed water ($H_2{}^{16}O$ and $D_2{}^{16}O$) molecules being the direct source of oxygen-containing species involved in the oxidation of methanol.[102] On the basis of transition-state theory, the observation of a kinetic isotope effect in a reaction suggests that the isotopic specie is directly involved in the rate-determining step.[103] Our current results provide strong evidence that water interacts with adsorbed oxygen to form OH and OD groups, which then react with impinging CO molecules to form CO_2.

(102) Wieckowski, A. *J. Electroanal. Chem.* **1977**, *78*, 229.
(103) Melander, L.; Saunders, W. H. J. *Reaction Rates of Isotopic Molecules*, 2nd ed.; Wiley: New York, 1980.

Conclusions

Previous studies have proposed that although water promotes CO oxidation, it is not directly involved in the reaction. However, we have presented unambiguous experimental evidence supported by DFT results that water promotes CO oxidation on Au(111) by directly reacting with adsorbed oxygen adatoms to form OH groups, followed by OH reacting with CO to form CO_2.

The initial step in this reaction is the interaction of water with oxygen atoms preadsorbed on Au(111). We observed that water strongly interacts with oxygen atoms leading to the activation of water to form a water−oxygen complex or hydroxyls, as evidenced by a new TPD feature with its peak near 175 K, in addition to the water desorption feature at 155 K, which is characteristic of water desorption without oxygen preadsorbed on the Au(111) surface. Supporting evidence from DFT calculations show that hydroxyls are readily formed by water on oxygen-precovered Au(111) because of the small activation barrier of 0.11 eV. Water−oxygen interactions also produce oxygen scrambling on the Au(111) surface, as evidenced from isotopic mixing in the oxygen evolution in TPD measurements. Here, oxygen atoms from adsorbed water exchange with adsorbed oxygen adatoms on the Au(111) surface, likely because of rapid diffusion of OH groups with subsequent reversible reactions between two nearby adsorbed hydroxyl groups to adsorbed water and oxygen.

We noted that labeled oxygen from water, for example $H_2{}^{18}O$, is observed as evolving $^{18}OC^{16}O$ after $C^{16}O$ impingement on a Au(111) surface covered with both oxygen and isotopically labeled water, suggesting that water is directly involved in the oxidation of CO on this surface. DFT calculations also showed that in the presence of H_2O, the barrier for CO oxidation for a select pathway is reduced to 0.11 eV, compared to 0.25 eV for CO oxidation on oxygen-precovered Au(111) without H_2O. This reduction is attributed to a concerted hydrogen transfer from one hydroxyl to another that acts to stabilize the transition state for CO oxidation and promote CO oxidation at temperatures as low as 45 K. However, DFT calculations suggest that more than one reaction pathway is involved in the oxidation of CO by Au(111) with coadsorbed oxygen adatoms and water because experimentally, we observe that 70−80% of that water is consumed in this reaction.

Finally, kinetic isotope effects were observed in water−oxygen interactions as well as in water-enhanced CO oxidation with $H_2{}^{16}O$, showing higher reactivity than $D_2{}^{16}O$ in both cases. On the basis of all these results, we propose that OH or OD groups formed from water interacting with atomic oxygen on Au(111) are responsible for the promotional effect in oxidizing CO to produce CO_2 on the surface.

Acknowledgment. The authors thank the Department of Energy (DE-FG02-04ER15587), Welch Foundation (F-1436 and F-1601), and National Science Foundation (CTS-0553243 and CHE-0645497) for their generous support of this research. C.B.M. also acknowledges the donors of the Petroleum Research Fund, administered by the American Chemical Society, for their financial support of this work. J.L.G. thanks the International Precious Metal Institute for a student award.

JA800351J

J|A|C|S COMMUNICATIONS

Published on Web 08/02/2008

Carbonate Formation and Decomposition on Atomic Oxygen Precovered Au(111)

Rotimi A. Ojifinni, Jinlong Gong, Nathan S. Froemming, David W. Flaherty, Ming Pan, Graeme Henkelman, and C. Buddie Mullins*

University of Texas at Austin, Departments of Chemical Engineering and Chemistry, Center for Nano- and Molecular Science and Technology, and Texas Materials Institute, 1 University Station C0400, Austin, Texas 78712-0231

Received May 9, 2008; E-mail: Mullins@che.utexas.edu

The carbonate formation and decomposition ($CO_3 \leftrightarrow CO_2 + O_a$) reaction on gold is important from the point of view of low-temperature CO oxidation. Carbonate formation has been proposed as a possible reaction intermediate in CO oxidation in several investigations of supported and unsupported gold clusters.[1−4] Therefore, an understanding of this reaction on Au(111) may provide additional insight. Carbonate formation and decomposition went undetected in previous studies on Au(110)[5] and Au(111).[6] However, a surface carbonate was readily formed when oxygen precovered Ag(110) was exposed to CO_2 at 300 K.[7−10] This surface carbonate decomposes to produce CO_2 at 485 K and the remaining oxygen atoms recombinatively desorbed at 590 K.[7−10] Owing to its similarity with silver, we would anticipate equally facile carbonate formation and decomposition reactions on gold. Similar reactions have also been reported on other surfaces.[11−13]

Here we present experimental evidence with supporting density functional theory (DFT) calculations of carbonate formation and decomposition from the adsorption of oxygen-labeled carbon dioxide ($C^{18}O_2$) on an atomic oxygen (^{16}O) precovered Au(111) surface. We studied the effects of CO_2 exposure, surface temperature, and oxygen coverage on carbonate formation and decomposition and also estimated reaction probabilities ($\sim 10^{-3}-10^{-4}$) and activation energies as a function of conditions.

Our experiments were performed in a UHV chamber that has been described elsewhere,[14−19] but details specific to this study are briefly summarized here. The Au(111) single crystal sample is mounted to a tantalum plate that can be resistively heated and is in thermal contact with a liquid nitrogen bath. Oxygen (^{16}O) atoms were deposited using a radio frequency (RF) plasma-jet source. The $^{16}O_a$/Au(111) surface was exposed to $C^{18}O_2$ by backfilling the chamber and carbonate $^{16}OC^{18}O^{18}O$ was formed. The surface carbonate decomposes to form either $C^{18}O_2$ or ^{16}O $C^{18}O$ leaving $^{18}O_a$ or $^{16}O_a$ adatoms on the surface. Upon heating, the oxygen atoms undergo recombinative desorption to produce $^{16}O_2$ (mass 32) and $^{16}O^{18}O$ (mass 34), as observed in TPD. Thus, carbonate formation and decomposition were detected via the increased presence of mass 34 $^{18}O^{16}O$ in a temperature programmed desorption (TPD) spectrum after the $^{16}O_a$ covered Au(111) surface was exposed to $C^{18}O_2$. We did not observe $^{18}O_2$ (mass 36) in TPD due to the very small surface concentration of ^{18}O. This method was employed after other strategies proved unsuccessful because of the low reaction probability.

Figure 1a displays TPD spectra of $^{16}O^{18}O$ ($m/e = 34$) produced from exposure of the $^{16}O_a$/Au(111) surface to $C^{18}O_2$. The amount of $^{16}O^{18}O$ produced increases with $C^{18}O_2$ exposure at 167 K (and all temperatures studied). Two control experiments were performed to ascertain the source of $^{16}O^{18}O$. First, no mass 34 was produced when the Au(111) surface was exposed to $C^{18}O_2$ *without* pre-adsorbed atomic oxygen. Second, only ~0.5% of the total amount

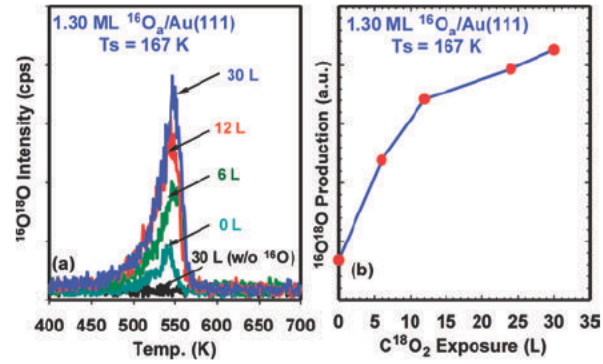

Figure 1. (a) TPD of $^{16}O^{18}O$ ($m/e = 34$) after a Au(111) surface covered with 1.3 ML ^{16}O at 77 K was exposed to varying amounts (0−30 L, where $1\ L = 10^{-6}$ Torr·s) of $C^{18}O_2$ at 167 K; (b) $^{16}O^{18}O$ production as a function of $C^{18}O_2$ exposure.

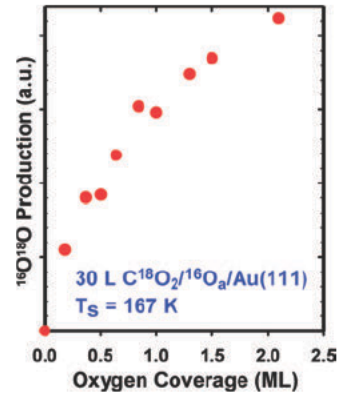

Figure 2. Integrated TPD area of $^{16}O^{18}O$ (mass 34) for varying initial oxygen precoverages (0.18−2.1 ML) on which 30 L of $C^{18}O_2$ was reacted at 167 K. The contribution to the signal due to the natural abundance of ^{18}O has been subtracted off.

of oxygen desorbs as mass 34 when the Au(111) surface is precovered with ^{16}O but with no exposure to $C^{18}O_2$ (due to natural isotopic abundance of ^{18}O). As expected, no surface-bound oxygen was lost during carbonate formation and decomposition, in agreement with previous studies.[8−10] Figure 1b shows the amount of mass 34 produced (from the spectra in Figure 1a) as a function of $C^{18}O_2$ exposure.

To further examine the role of preadsorbed atomic oxygen on carbonate formation, we varied the oxygen precoverage (0.18−2.1 ML) while keeping both $C^{18}O_2$ exposure (30 L) and surface temperature (167 K) constant (Figure 2). Mass 34 production increases with increasing $^{16}O_a$ coverage, likely because more reactive oxygen is accessible to $C^{18}O_2$ on the surface. Similar results were obtained employing surface temperatures of 220 and 300 K.

10.1021/ja803482h CCC: $40.75

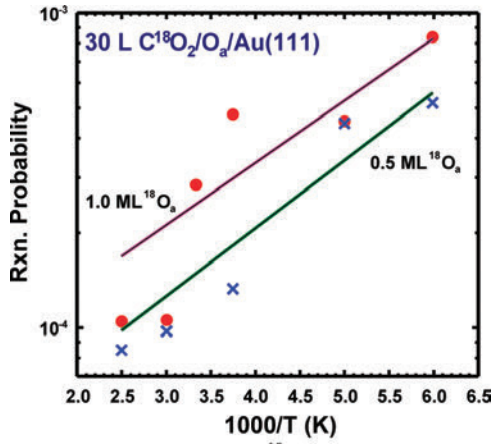

Figure 3. Arrhenius plot of $C^{18}O_2$ reaction probability using a constant $C^{18}O_2$ exposure of 30 L for 1.0 ML (upper plot) and 0.5 ML (lower plot) of atomic oxygen on Au(111).

We estimated the reaction probability of carbonate formation assuming a statistical distribution[7] in the decomposition of the surface-bound carbonate $^{16}OC^{18}O_2$ and obtained values of $\sim 10^{-3}-10^{-4}$ (uncertainties of $\pm 50\%$). These small values are likely part of the reason why an earlier study on Au(111)[6] reported undetectable surface carbonate formation. An Arrhenius plot of the reaction probability for two oxygen coverages (0.5 and 1.0 ML) is shown in Figure 3. The inverse relationship between reaction probability and temperature, with negative apparent activation energy $E_a = -0.15 \pm 0.08$ eV, is suggestive of a competition between carbonate formation and $C^{18}O_2$ desorption on the O/Au(111) surface.

Compared to Au(111), the carbonate formation reaction on Ag(110) is very facile.[10] This difference is not currently understood but could be related to surface structure or other factors (likely not entirely due to the calculated energetics described below). Using DFT we have calculated the difference in energetics for CO_3 formation on Au(111), Au(110), Ag(111), and Ag(110). The metal surfaces were modeled with 4 (for 111) and 6 (for 110) layers, allowing the top two layers to relax. A vacuum gap of 10 Å separated the slabs. A plane wave basis set with a 274 eV cutoff was found to be sufficient for the PAW-based pseudopotentials,[20] with a $4 \times 4 \times 1$ Monkhost-Pack k-point sampling of the Brillouin zone. All calculations were based upon the PW91 GGA functional.[21]

Figure 4 shows calculated reaction paths for CO_3 formation on the metal surfaces. The initial point on each path corresponds to the binding of a single O atom at the most stable site on the surface, with the zero of energy taken with respect to gas-phase CO_2 and $^1/_2O_2$. CO_2 physisorbs to O_a and the two can react to form CO_3. The formation of CO_3 on Ag(110) was found to be spontaneous, and it occurs with only a very small barrier of 0.04 eV on Ag(111). For Au, however, there is a significant barrier to CO_3 formation, particularly on the (111) surface. Our calculations show that CO_3 is bound much more strongly to Ag than to Au, consistent with our experimental results on Au(111) in which CO_3 decomposition and CO_2 desorption appear to occur in an overlapping temperature range (90−120 K) while on Ag(110), the carbonate decomposes near 485 K and CO_2 desorbs below 160 K.

Our DFT calculations are consistent with the observed low reaction probability on Au(111) since CO_3 formation is activated as compared to CO_2 desorption. They do not explain the apparent negative activation energy; additional calculations including surface reconstructions may be necessary.

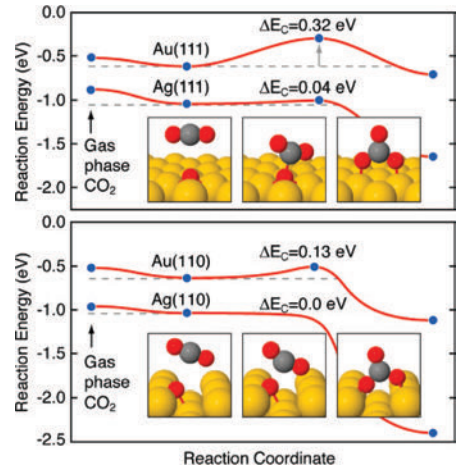

Figure 4. DFT calculations of carbonate formation on Au and Ag (111, upper plot) and (110, lower plot) surfaces. Energy barriers, ΔE_c, are labeled for each reaction pathway.

In summary, we have shown evidence for carbonate formation and reaction on atomic oxygen precovered Au(111). Oxygen mixing was observed when $^{16}O_a$ precovered Au(111) was exposed to isotopically labeled CO_2 ($C^{18}O_2$) at surface temperatures ranging from 77−400 K and initial oxygen coverages ranging from 0.18−2.1 ML. Subsequent desorption of isotopically mixed oxygen ($^{16}O^{18}O$, mass 34) is observed as a byproduct of carbonate formation and decomposition on the surface. Carbonate formation occurs with a very small reaction probability (ca. $10^{-3}-10^{-4}$) and is most favorable at low surface temperatures.

Acknowledgment. We acknowledge the Department of Energy (DE-FG02-04ER15587), Welch Foundation (F-1436; F-1601), National Science Foundation (CTS-0553243; CHE-0645497) and the donors of the Petroleum Research Fund, administered by the American Chemical Society, for their support.

References

(1) Date, M.; Haruta, M. *J. Catal.* **2001**, *201*, 221.
(2) Daté, M.; Okumura, M.; Tsubota, S.; Haruta, M. *Angew. Chem., Int. Ed.* **2004**, *43*, 2129.
(3) Hakkinen, H.; Landman, U. *J. Am. Chem. Soc.* **2001**, *123*, 9704.
(4) Konova, P.; Naydenov, A.; Venkov, C.; Mehandjiev, D.; Andreeva, D.; Tabakova, T. *J. Mol. Catal. A* **2004**, *213*, 235.
(5) Outka, D. A.; Madix, R. J. *Surf. Sci.* **1987**, *179*, 351.
(6) Lazaga, M. A.; Wickham, D. T.; Parker, D. H.; Kastanas, G. N.; Koel, B. E. *ACS Symp. Ser.* **1993**, *523*, 90.
(7) Barteau, M. A.; Madix, R. J. *J. Chem. Phys.* **1981**, *74*, 4144.
(8) Bowker, M.; Barteau, M. A.; Madix, R. J. *Surf. Sci.* **1980**, *92*, 528.
(9) Campbell, C. T.; Paffett, M. T. *Surf. Sci.* **1984**, *143*, 517.
(10) Guo, X. C.; Madix, R. J. *J. Phys. Chem. B* **2001**, *105*, 3878.
(11) Behm, R. J.; Brundle, C. R. *Surf. Sci.* **1991**, *255*, 327.
(12) Felter, T. E.; Weinberg, W. H.; Lastushkina, G. Y.; Boronin, A. I.; Zhdan, P. A.; Boreskov, G. K.; Hrbek, J. *Surf. Sci.* **1982**, *118*, 369.
(13) Wang, Y.; Kovacik, R.; Meyer, B.; Kotsis, K.; Stodt, D.; Staemmler, V.; Qiu, H.; Traeger, F.; Langenberg, D.; Muhler, M.; Woll, C. *Angew. Chem., Int. Ed.* **2007**, *46*, 5624.
(14) Ojifinni, R. A.; Froemming, N. S.; Gong, J. L.; Pan, M.; Kim, T. S.; White, J. M.; Henkelman, G.; Mullins, C. B. *J. Am. Chem. Soc.* **2008**, *130*, 6801.
(15) Stiehl, J. D.; Kim, T. S.; McClure, S. M.; Mullins, C. B. *J. Am. Chem. Soc.* **2004**, *126*, 13574.
(16) Stiehl, J. D.; Kim, T. S.; McClure, S. M.; Mullins, C. B. *J. Am. Chem. Soc.* **2004**, *126*, 1606.
(17) Kim, T. S.; Gong, J.; Ojifinni, R. A.; White, J. M.; Mullins, C. B. *J. Am. Chem. Soc.* **2006**, *128*, 6282.
(18) Gong, J.; Ojifinni, R. A.; Kim, T. S.; White, J. M.; Mullins, C. B. *J. Am. Chem. Soc.* **2006**, *128*, 9012.
(19) Wheeler, M. C.; Seets, D. C.; Mullins, C. B. *J. Chem. Phys.* **1996**, *105*, 1572.
(20) Kresse, G.; Joubert, D. *Phys. Rev. B.* **1999**, *59*, 1758.
(21) Perdew, J. P. In *Electronic Structure of Solids '91*; Ziesche, P., Eschrig, H., Eds.; Akademie Verlag: Berlin, 1991; pp 11−20..

JA803482H